

Univerza
v Ljubljani
Fakulteta
*za gradbeništvo
in geodezijo*



Jamova 2
1000 Ljubljana, Slovenija
<http://www3.fgg.uni-lj.si/>

DRUGG – Digitalni repozitorij UL FGG
<http://drugg.fgg.uni-lj.si/>

Ta članek je avtorjeva zadnja recenzirana različica, kot je bila sprejeta po opravljeni recenziji.

Prosimo, da se pri navajanju sklicujete na bibliografske podatke, kot je navedeno:

University
of Ljubljana
Faculty of
*Civil and Geodetic
Engineering*



Jamova 2
SI – 1000 Ljubljana, Slovenia
<http://www3.fgg.uni-lj.si/>

DRUGG – The Digital Repository
<http://drugg.fgg.uni-lj.si/>

This version of the article is author's manuscript as accepted for publishing after the review process.

When citing, please refer to the publisher's bibliographic information as follows:

Brank, B., Korelc, J., 2003. Dynamics and Time-Stepping Schemes for Elastic Shells Undergoing Finite Rotations. *Computers & Structures*. 81, 12: 1193–1210.

<http://www.sciencedirect.com/science/article/pii/S0045794903000361>

Dynamics and Time-Stepping Schemes for Elastic Shells Undergoing Finite Rotations

Boštjan Brank, Jože Korelc

University of Ljubljana, Faculty of Civil and Geodetic Engineering

Jamova 2, 1000 Ljubljana, Slovenia

e-mails: bbrank@fgg.uni-lj.si; jkorelc@fgg.uni-lj.si

Adnan Ibrahimbegović

Ecole Normale Supérieure de Cachan/LMT

61, av. du président Wilson, 94235 Cachan cedex, France

e-mail: Adnan.Ibrahimbegovic@lmt.ens-cachan.fr

May 30, 2012

Abstract

In this work we study the time-stepping schemes for shell models which describe the shell director vector motion by the finite rotations. Different possibilities for choosing director rotations are examined and their relationships are cast in terms of the commutative diagram. The Newmark time-stepping schemes, making use of different rotation parameters, are then developed. The mid-point scheme modified to either conserve or dissipate the total energy is further examined. Several numerical simulations are presented to illustrate the performance of each developed scheme.

Key words: shells, finite rotations, nonlinear dynamics, finite elements, time-stepping schemes

1. Introduction

Thin shell structures can find very interesting applications in civil, mechanical or aerospace engineering as an optimal structural form allowing for the most efficient use of a given material. Slender thin shells will in general experience motion with large displacements and large rotations, while the strains will be usually left small allowing us to model linear elastic constitutive equations. The shell problem complexity thus stems mostly from the nonlinear kinematics of large rotations.

Of particular interest of this work are applications in dynamics of shells. Examples are wind or earthquake loading induced shell vibrations or snap-through instability phenomena, which ought to be placed within the context of dynamics to provide proper interpretation. In short, we herein deal with nonlinear dynamics of elastic shells undergoing large rotations. The time-stepping solution is often the only way to solve such problems.

The nonlinear behavior of thin shell can be captured by the Cosserat surface theory (e.g. see Naghdi [19]), which is assumed to be a smooth surface with a so-called director vector attached at each point. The small strain assumption is further corroborated by assuming that shell remains of constant thickness and that the director vector can be chosen as an inextensible unit vector indicating the current position of the corresponding fiber. The large rotation of a unit vector can be fully mastered by exploiting the analogy with the space of constrained rotation tensors (e.g. see Simo and Fox [23]), which allows one to construct singularity-free large rotations updates. This kind of analogy can be developed further (e.g. see Ibrahimbegović, Brank and Courtois [15]) in order to provide a computationally more convenient additive rotation updates which remain singularity-free. Contrary to the works using Euler angles (e.g. see Ramm and Matzenmiller [20], Hughes and Pister [9]) we employ the incremental rotation vector

In this work we present a detailed analysis of different choices for rotation vector parameters (e.g. Ibrahimbegović [13], Brank and Ibrahimbegović [7], Betsch, Menzel and Stein [3]) to bear on the problem of constructing the most suitable for the standard Newmark time-stepping scheme when applied to shells. Moreover, we examine an alternative time-stepping scheme based on mid-point rule and pertinent modifications of that scheme designed to either conserve or decay the total energy. The main idea is to modify the computation of the algorithmic stress resultants and the velocity updates so that the energy can be either conserved or decayed in a controllable manner. The energy decaying scheme is an extension of the energy conserving scheme for shells proposed by Simo and Tarnow [24], and further elaborated by Kuhl and Ramm [18], Sansour, Wriggers and Sansour [21], Brank, Briseghella, Tonello and Damjanić [6], Bottaso, Bauchau and Choi [4], and others. Majority of these works is related to the extensional shell-director models consequently avoiding large rotation complexities.

The outline of the paper is as follows. In Section 2 we briefly present the equations governing the nonlinear dynamics of the chosen shell model. In Section 3 we discuss construction of the corresponding constrained finite rotation. Two families of time-stepping schemes, Newmark and mid-point, are discussed in Section 4. Several numerical examples presented in Section 5, are followed by conclusions in Section 6.

2. Dynamics of geometrically exact shell

We begin with a brief account of the evolution equations governing nonlinear dynamics of shell undergoing large displacements and rotations. The chosen shell model represents a single director Cosserat surface (see e.g. Naghdi [19], Simo and Fox [23] or Ibrahimbegović [12]) with the position vector in a shell deformed configuration assumed to be defined as

$$\boldsymbol{\varphi}(\xi^1, \xi^2, t) + \zeta \mathbf{t}(\xi^1, \xi^2, t); \quad (\xi^1, \xi^2) \in \mathcal{A}; \quad \zeta \in \mathcal{F} := \{h^-, h^+\} \quad (2.1)$$

In (2.1) above \mathcal{A} defines the domain of the mid-surface parametrization, $h = h^+ - h^-$ is the thickness of the shell, ξ^1 and ξ^2 are convected curvilinear coordinates, ζ is through-the-thickness coordinate and t is time parameter defined within the interval of interest $t \in [t_0, T]$. It is assumed that the director vector \mathbf{t} is a unit vector. It thus follows from (2.1) that all deformed configurations of the shell are determined by pairs $(\boldsymbol{\varphi}, \mathbf{t})$ and that the configuration space is

defined by

$$\mathcal{C} := \left\{ (\boldsymbol{\varphi}, \mathbf{t}) : \mathcal{A} \rightarrow \mathbb{R}^3 \times S^2 \mid \boldsymbol{\varphi}|_{\partial\mathcal{A}_\varphi} = \bar{\boldsymbol{\varphi}}, \mathbf{t}|_{\partial\mathcal{A}_t} = \bar{\mathbf{t}} \right\} \quad (2.2)$$

Here S^2 is a unit sphere, while $\partial\mathcal{A}_\varphi$ and $\partial\mathcal{A}_t$ are parts of the boundary where the displacement and the director field are specified, respectively. The shell initial configuration is defined by a pair $(\boldsymbol{\varphi}_0, \mathbf{t}_0)$.

The kinematic equations of the shell are then developed as follows. We define at each point of the mid-surface the convected frame $\{\mathbf{t}_i\}$, which is obtained by mapping of the frame $\{\mathbf{g}_i\}$ constructed at time t_0 (see Figure 1)

$$\{\mathbf{t}_1, \mathbf{t}_2, \mathbf{t}_3\} := \{\boldsymbol{\varphi}_{,1}, \boldsymbol{\varphi}_{,2}, \mathbf{t}\}; \quad \{\mathbf{g}_1, \mathbf{g}_2, \mathbf{g}_3\} := \{\boldsymbol{\varphi}_{0,1}, \boldsymbol{\varphi}_{0,2}, \mathbf{t}_0\} \quad (2.3)$$

where $(\circ)_{,\alpha} \equiv \frac{\partial}{\partial \xi^\alpha}(\circ)$. It is assumed that the director vector is initially orthogonal to the shell mid-surface, but it need not remain orthogonal to the deformed mid-surface, which allows us to account for shear deformation. The relative deformation gradient at $\boldsymbol{\varphi}_0$ is a linear map $\mathbf{F} : T_{\boldsymbol{\varphi}_0}\mathcal{C} \rightarrow T_\varphi\mathcal{C}$, given as

$$\mathbf{F} = \mathbf{t}_i \otimes \mathbf{g}^i = \mathbf{t}_\alpha \otimes \mathbf{g}^\alpha + \mathbf{t}_3 \otimes \mathbf{t}_0 \quad (2.4)$$

where \mathbf{g}^α are the dual base vectors ($\mathbf{g}^\alpha \cdot \mathbf{g}_\beta = \delta_\beta^\alpha$). The Green-Lagrange strain measures for the shell may then be defined as

$$\mathbf{E}^{m,s} = \frac{1}{2} [\mathbf{F}^T \mathbf{F} - \mathbf{1}] \quad (2.5)$$

where $\mathbf{1}$ is a unit tensor relative to the reference configuration. It follows from (2.4) and (2.5) that the components of the strain tensor $\mathbf{E}^{m,s}$ in the \mathbf{g}^i basis can be written as

$$\varepsilon_{\alpha\beta} = \frac{1}{2} (\boldsymbol{\varphi}_{,\alpha} \cdot \boldsymbol{\varphi}_{,\beta} - \boldsymbol{\varphi}_{0,\alpha} \cdot \boldsymbol{\varphi}_{0,\beta}); \quad 2\varepsilon_{\alpha 3} = \gamma_\alpha = \boldsymbol{\varphi}_{,\alpha} \cdot \mathbf{t} - \boldsymbol{\varphi}_{0,\alpha} \cdot \mathbf{t}_0 \quad (2.6)$$

where $\varepsilon_{\alpha\beta}$ and γ_α are the classical expressions for the membrane and the shear strains; e.g. see Naghdi [19]. The Green-Lagrange strain measures for the bending strains can be developed by making use of the director gradient, defined as the $\mathbf{G} = \mathbf{t}_{,\alpha} \otimes \mathbf{g}^\alpha$, which allows us to write

$$\mathbf{E}^b = \mathbf{F}^T \mathbf{G} - \mathbf{B} \quad (2.7)$$

where $\mathbf{B} = (\mathbf{g}_\alpha \cdot \mathbf{g}_{,\beta}) \mathbf{g}^\alpha \otimes \mathbf{g}^\beta$ is the curvature tensor in the initial configuration. The components of the strain tensor \mathbf{E}^b in the \mathbf{g}^i basis can be written as

$$\kappa_{\alpha\beta} = \boldsymbol{\varphi}_{,\alpha} \cdot \mathbf{t}_{,\beta} - \boldsymbol{\varphi}_{0,\alpha} \cdot \mathbf{t}_{0,\beta} \quad (2.8)$$

which are the classical expressions for the shell bending strains; e.g. see Naghdi [19].

In order to specify the constitutive behavior of the shell with the strain measures (2.6) and (2.8), we can define the strain energy function

$$\Phi(\varepsilon_{\alpha\beta}, \gamma_\alpha, \kappa_{\alpha\beta}, \diamond) \quad (2.9)$$

An empty slot in (2.9) indicates that such a strain energy function should also depend in general upon the first and the second fundamental forms of the mid-surface. The effective stress resultants can be obtained as the corresponding partial derivatives of the strain energy, i.e.

$$n^{\alpha\beta} = \frac{\partial\Phi}{\partial\varepsilon_{\alpha\beta}}; \quad q^\alpha = \frac{\partial\Phi}{\partial\gamma_\alpha}; \quad m^{\alpha\beta} = \frac{\partial\Phi}{\partial\kappa_{\alpha\beta}} \quad (2.10)$$

where $n^{\alpha\beta}$ and q^α are effective membrane and shear stress resultants and $m^{\alpha\beta}$ are couples. The simplest properly invariant constitutive relations for shells are obtained by postulating the linear elastic and isotropic response and by neglecting a variation of metric tensor through the shell thickness which leads to a quadratic form of the strain energy given as:

$$n^{\alpha\beta} = \frac{Eh}{1-\nu^2} H^{\alpha\beta\gamma\delta} \varepsilon_{\gamma\delta}; \quad m^{\alpha\beta} = \frac{Eh^3}{12(1-\nu^2)} H^{\alpha\beta\gamma\delta} \kappa_{\gamma\delta}; \quad q^\alpha = \varkappa Gh g^{\alpha\beta} \gamma_\beta \quad (2.11)$$

where E is Young's modulus, G is shear modulus, ν is Poisson's ratio, \varkappa is shear correction factor, $g^{\alpha\beta} = \mathbf{g}^\alpha \cdot \mathbf{g}^\beta$, and

$$H^{\alpha\beta\gamma\delta} = \nu g^{\alpha\beta} g^{\gamma\delta} + \frac{1}{2} (1-\nu) (g^{\alpha\gamma} g^{\beta\delta} + g^{\alpha\delta} g^{\beta\gamma}) \quad (2.12)$$

In order to complete the description of the chosen shell problem we write the two-dimensional momentum balance equations in the vector form (e.g. Simo and Fox [23])

$$A_{\bar{\rho}} \ddot{\boldsymbol{\varphi}} = \frac{1}{\sqrt{a}} (\sqrt{a} \mathbf{n}^\alpha)_{,\alpha} + \bar{\mathbf{n}}; \quad I_{\bar{\rho}} (\mathbf{t} \times \ddot{\mathbf{t}}) = \frac{1}{\sqrt{a}} (\sqrt{a} \mathbf{m}^\alpha)_{,\alpha} + \boldsymbol{\varphi}_{,\alpha} \times \mathbf{n}^\alpha + \bar{\mathbf{m}} \quad (2.13)$$

where \mathbf{n}^α and \mathbf{m}^α are stress resultant and stress couple vectors¹, $\bar{\mathbf{n}}$ and $\bar{\mathbf{m}}$ are the applied external force and couple, respectively, and $\sqrt{a} = \|\mathbf{t}_1 \times \mathbf{t}_2\|$ is the surface Jacobian at the deformed configuration; $a = \det[\mathbf{t}_\alpha \cdot \mathbf{t}_\beta]$. In (2.13) above $A_{\bar{\rho}}$ and $I_{\bar{\rho}}$ are the surface mass density and the rotation inertia of the shell-director at the deformed configuration, respectively. In the spirit of d'Alambert principle, we can derive the corresponding weak form of the balance equations by introducing the inertia forces, multiplying the equations by test functions $\delta\boldsymbol{\varphi}$ and $\delta\mathbf{t}$ and making use of the integration by parts; e.g. see Hughes [10]. The weak form of the equations of motion can then be written with respect to the reference configuration as

$$\delta\Sigma(\boldsymbol{\varphi}, \mathbf{t}, \delta\boldsymbol{\varphi}, \delta\mathbf{t}) = \int_A (A_\rho \ddot{\boldsymbol{\varphi}} \cdot \delta\boldsymbol{\varphi} + I_\rho \ddot{\mathbf{t}} \cdot \delta\mathbf{t}) dA + \delta\Pi(\boldsymbol{\varphi}, \mathbf{t}, \delta\boldsymbol{\varphi}, \delta\mathbf{t}) = \delta K + \delta\Pi = 0 \quad (2.14)$$

where δK is the variation of the shell kinetic energy, and

$$A_\rho = \frac{\sqrt{a}}{\sqrt{g}} A_{\bar{\rho}} = \rho h; \quad I_\rho = \frac{\sqrt{a}}{\sqrt{g}} I_{\bar{\rho}} = \frac{\rho h^3}{12} \quad (2.15)$$

¹The components of \mathbf{n}^α are $n^{\alpha\beta}$ and $n^{\alpha 3} = q^\alpha$, whereas the components of \mathbf{m}^α are $m^{\alpha\beta}$ and $m^{\alpha 3} = 0$.

where \sqrt{g} and ρ are the surface Jacobian and the 3-d mass density at the initial configuration. In (2.14) above $\delta\Pi$ is the weak form of the static equilibrium equations which can be written as

$$\begin{aligned} \delta\Pi(\boldsymbol{\varphi}, \mathbf{t}, \delta\boldsymbol{\varphi}, \delta\mathbf{t}) &= \int_A \left[n^{\alpha\beta} \frac{1}{2} (\delta\boldsymbol{\varphi}_{,\alpha} \cdot \boldsymbol{\varphi}_{,\beta} + \boldsymbol{\varphi}_{,\alpha} \cdot \delta\boldsymbol{\varphi}_{,\beta}) + q^\alpha (\delta\boldsymbol{\varphi}_{,\alpha} \cdot \mathbf{t} + \boldsymbol{\varphi}_{,\alpha} \cdot \delta\mathbf{t}) \right. \\ &+ \left. \int_A m^{\alpha\beta} (\delta\boldsymbol{\varphi}_{,\alpha} \cdot \mathbf{t}_{,\beta} + \boldsymbol{\varphi}_{,\alpha} \cdot \delta\mathbf{t}_{,\beta}) \right] dA - \delta\Pi_{ext}(\boldsymbol{\varphi}, \mathbf{t}, \delta\boldsymbol{\varphi}, \delta\mathbf{t}) \end{aligned} \quad (2.16)$$

where the terms multiplied with the membrane and the shear stress resultants and the couples (2.10) are variations of strains given in (2.6) and (2.8), and $\delta\Pi_{ext}$ is the virtual work of the applied external forces.

For the shell problem with an elastic behavior considered herein, the weak form in (2.14) can also be obtained as the first variation of the total energy, which, in accordance with (2.9), can be written as

$$\Sigma(\boldsymbol{\varphi}, \mathbf{t}) = \Pi(\boldsymbol{\varphi}, \mathbf{t}) + K(\boldsymbol{\varphi}, \mathbf{t}) \quad (2.17)$$

$$\Pi(\boldsymbol{\varphi}, \mathbf{t}) = \int_A \Phi(\varepsilon_{\alpha\beta}, \gamma_\alpha, \kappa_{\alpha\beta}, \circ) dA - \Pi_{ext}(\boldsymbol{\varphi}, \mathbf{t}) \quad (2.18)$$

$$K(\boldsymbol{\varphi}, \mathbf{t}) = \frac{1}{2} \int_A [A_\rho \dot{\boldsymbol{\varphi}} \cdot \dot{\boldsymbol{\varphi}} + I_\rho \dot{\mathbf{t}} \cdot \dot{\mathbf{t}}] dA \quad (2.19)$$

where Π and K are, respectively, the total potential and the total kinetic energy of the shell.

In solving this highly nonlinear problem of shell dynamics at finite rotations we make use of the Newton incremental-iterative method, which solves successively in each iteration the linearized form of equation (2.14) given as

$$\begin{aligned} \text{Lin}[\delta\Sigma(\cdot)] &= [\delta\Sigma(\cdot)] \\ &+ \int_A \left[\frac{1}{2} (\delta\boldsymbol{\varphi}_{,\alpha} \cdot \boldsymbol{\varphi}_{,\beta} + \boldsymbol{\varphi}_{,\alpha} \cdot \delta\boldsymbol{\varphi}_{,\beta}) \frac{\partial^2 \Phi}{\partial \varepsilon_{\alpha\beta} \partial \varepsilon_{\gamma\delta}} \frac{1}{2} (\Delta\boldsymbol{\varphi}_{,\gamma} \cdot \boldsymbol{\varphi}_{,\delta} + \boldsymbol{\varphi}_{,\gamma} \cdot \Delta\boldsymbol{\varphi}_{,\delta}) \right. \\ &+ (\delta\boldsymbol{\varphi}_{,\alpha} \cdot \mathbf{t} + \boldsymbol{\varphi}_{,\alpha} \cdot \delta\mathbf{t}) \frac{\partial^2 \Phi}{\partial \gamma_\alpha \partial \gamma_\beta} (\Delta\boldsymbol{\varphi}_{,\beta} \cdot \mathbf{t} + \boldsymbol{\varphi}_{,\beta} \cdot \Delta\mathbf{t}) \\ &+ (\delta\boldsymbol{\varphi}_{,\alpha} \cdot \mathbf{t}_{,\beta} + \boldsymbol{\varphi}_{,\alpha} \cdot \delta\mathbf{t}_{,\beta}) \frac{\partial^2 \Phi}{\partial \kappa_{\alpha\beta} \partial \kappa_{\gamma\delta}} (\Delta\boldsymbol{\varphi}_{,\gamma} \cdot \mathbf{t}_{,\delta} + \boldsymbol{\varphi}_{,\gamma} \cdot \Delta\mathbf{t}_{,\delta}) \left. \right] dA \\ &+ \int_A [n^{\alpha\beta} (\delta\boldsymbol{\varphi}_{,\alpha} \cdot \Delta\boldsymbol{\varphi}_{,\beta}) \\ &+ q^\alpha (\delta\boldsymbol{\varphi}_{,\alpha} \cdot \Delta\mathbf{t} + \Delta\boldsymbol{\varphi}_{,\alpha} \cdot \delta\mathbf{t}) \\ &+ m^{\alpha\beta} (\delta\boldsymbol{\varphi}_{,\alpha} \cdot \Delta\mathbf{t}_{,\beta} + \Delta\boldsymbol{\varphi}_{,\alpha} \cdot \delta\mathbf{t}_{,\beta}) \\ &+ q^\alpha (\boldsymbol{\varphi}_{,\alpha} \cdot \Delta\delta\mathbf{t}) + m^{\alpha\beta} (\boldsymbol{\varphi}_{,\alpha} \cdot \Delta\delta\mathbf{t}_{,\beta})] dA \\ &+ \int_A (A_\rho \Delta\dot{\boldsymbol{\varphi}} \cdot \delta\boldsymbol{\varphi} + I_\rho \Delta\dot{\mathbf{t}} \cdot \delta\mathbf{t} + I_\rho \ddot{\mathbf{t}} \cdot \Delta\delta\mathbf{t}) dA = 0 \end{aligned} \quad (2.20)$$

Here $\Delta\boldsymbol{\varphi}$ is an incremental displacement vector and $\Delta\mathbf{t}$ is an incremental director vector. Note that $\Delta\delta\boldsymbol{\varphi}$ is zero, while $\Delta\delta\mathbf{t}$ is generally not, due to chosen rotation parametrization of the shell configuration space in (2.2), (e.g. see Ibrahimbegović, Brank and Courtois [15] and Brank and Ibrahimbegović [7] for discussion of these issues). The integrals given in (2.20) provide the basis for computing the material and the geometric part of the tangent stiffness and the tangent mass matrix, which provide jointly the tangent operator.

The spatial discretization of the problem is performed by using the isoparametric finite element approximations yet referred to as the continuum-consistent (e.g. see Ibrahimbegović [12]). They ensure that the linearization and discretisation of a nonlinear shell problem can be carried out in an arbitrary order leading always to the same end results. More precisely, we use the standard procedure (e.g. see Bathe [1] or Zienkiewicz and Taylor [25]) based on the parent element to approximate the shell geometry

$$\boldsymbol{\varphi}(\xi^1, \xi^2, t) = \sum_{a=1}^{n_{en}} N_a(\xi^1, \xi^2) \boldsymbol{\varphi}_a(t); \quad \mathbf{t}(\xi^1, \xi^2, t) = \sum_{a=1}^{n_{en}} N_a(\xi^1, \xi^2) \mathbf{t}_a(t) \quad (2.21)$$

where $N_a(\xi^1, \xi^2)$ are the corresponding shape functions for a shell element with n_{en} nodes, $(\xi^1, \xi^2) \in [-1, 1] \times [-1, 1]$ are natural coordinates, and $(\circ)_a$ is used to denote the corresponding nodal values. The virtual and incremental quantities at any time $t \in [0, T]$ are interpolated in the same manner with

$$\delta\boldsymbol{\varphi}(\xi^1, \xi^2) = \sum_{a=1}^{n_{en}} N_a(\xi^1, \xi^2) \delta\boldsymbol{\varphi}_a; \quad \delta\mathbf{t}(\xi^1, \xi^2) = \sum_{a=1}^{n_{en}} N_a(\xi^1, \xi^2) \delta\mathbf{t}_a \quad (2.22)$$

$$\Delta\boldsymbol{\varphi}(\xi^1, \xi^2) = \sum_{a=1}^{n_{en}} N_a(\xi^1, \xi^2) \Delta\boldsymbol{\varphi}_a; \quad \Delta\mathbf{t}(\xi^1, \xi^2) = \sum_{a=1}^{n_{en}} N_a(\xi^1, \xi^2) \Delta\mathbf{t}_a \quad (2.23)$$

$$\Delta\delta\mathbf{t}(\xi^1, \xi^2) = \sum_{a=1}^{n_{en}} N_a(\xi^1, \xi^2) \Delta\delta\mathbf{t}_a$$

The derivatives of the above interpolated functions with respect to time, t , or coordinates ξ^1 and ξ^2 may be easily obtained in order to write the discrete approximations of the weak form (2.14) or its linearized counterpart in (2.20). An exception to this is the interpolation of the transverse shear fields, which is based on the assumed strain method as suggested by Bathe and Dvorkin [2].

3. Finite rotations of the shell director

We consider a general motion of the director vector attached to a particular point of the shell mid-surface. Since \mathbf{t} is a unit vector, its position may be given by a finite rotation of the base vector $\mathbf{e} \equiv \mathbf{e}_3 = \{0, 0, 1\}^T$, thus having at time $t \neq t_0$ and time t_0

$$\mathbf{t} = \boldsymbol{\Lambda}\mathbf{e}; \quad \mathbf{t}_0 = \boldsymbol{\Lambda}_0\mathbf{e} \quad (3.1)$$

for the current and the initial configuration, respectively. In (3.1) $\boldsymbol{\Lambda} \in SO(3)$ is a rotation tensor defined as²

$$\boldsymbol{\Lambda} = \tilde{\boldsymbol{\Lambda}}(\boldsymbol{\vartheta}) = \exp[\boldsymbol{\Theta}] = \cos\vartheta\mathbf{I} + \frac{\sin\vartheta}{\vartheta}\boldsymbol{\Theta} + \frac{1 - \cos\vartheta}{\vartheta^2}\boldsymbol{\vartheta} \otimes \boldsymbol{\vartheta} \quad (3.2)$$

²We use notation $\tilde{\boldsymbol{\Lambda}}(\boldsymbol{\vartheta})$ to denote explicitly that $\boldsymbol{\Lambda}$ is a function of a rotation vector $\boldsymbol{\vartheta}$.

where $\boldsymbol{\vartheta}$ is an eigenvector of Λ (referred to as rotation vector, e.g. Ibrahimbegović, Frey and Kožar [11]) and $\Theta \mathbf{b} = \boldsymbol{\vartheta} \times \mathbf{b}$ for any $\mathbf{b} \in \mathbb{R}^3$. We assume that tensor Λ will rotate \mathbf{e} to \mathbf{t} without making use of the drilling rotation (e.g. see Ibrahimbegović, Brank and Courtois [15], Brank and Ibrahimbegović [7]). More precisely, rotation tensor Λ is constructed by requiring that the rotation vector component along the rotated vector plays no role in the theory, which can be expressed with

$$\boldsymbol{\vartheta} \cdot \mathbf{e} = 0; \quad \mathbf{t} \cdot \dot{\mathbf{t}} = 0 \quad (3.3)$$

The time derivation of the shell-director vector \mathbf{t} may be obtained as

$$\dot{\mathbf{t}} = \left. \frac{d}{dt} \right|_{t=0} \mathbf{t}_t = \left. \frac{d}{dt} \right|_{t=0} \Lambda_t \mathbf{e} \quad (3.4)$$

where \mathbf{t}_t and Λ_t represent the time evolution with respect to the shell deformed configuration. To compute the latter we multiply Λ from the right by an orthogonal tensor $\exp [t\dot{\Psi}]$

$$\mathbf{t}_t = \Lambda_t \mathbf{e} = \Lambda \exp [t\dot{\Psi}] \mathbf{e} \quad (3.5)$$

or we multiply Λ from the left by an orthogonal tensor $\exp [t\dot{\mathbf{W}}]$

$$\mathbf{t}_t = \Lambda_t \mathbf{e} = \exp [t\dot{\mathbf{W}}] \Lambda \mathbf{e} = \exp [t\dot{\mathbf{W}}] \mathbf{t} \quad (3.6)$$

where $\dot{\Psi}$ and $\dot{\mathbf{W}}$ are skew-symmetric tensors defining material and spatial angular velocities of the shell-director, respectively. Relationship between $\dot{\Psi}$ and $\dot{\mathbf{W}}$ and their axial vectors can easily be obtained (see Ibrahimbegović, Fray and Kožar [11])

$$\dot{\Psi} = \Lambda^T \dot{\mathbf{W}} \Lambda; \quad \dot{\mathbf{W}} = \Lambda \dot{\Psi} \Lambda^T; \quad \dot{\boldsymbol{\psi}} = \Lambda^T \dot{\mathbf{w}}; \quad \dot{\mathbf{w}} = \Lambda \dot{\boldsymbol{\psi}} \quad (3.7)$$

By using the results in (3.5) and (3.6) we get from (3.4) the following expressions for the shell-director velocity in terms of $\dot{\boldsymbol{\psi}}$ and $\dot{\mathbf{w}}$

$$\dot{\mathbf{t}} = \Lambda (\dot{\boldsymbol{\psi}} \times \mathbf{e}); \quad \dot{\mathbf{t}} = \dot{\mathbf{w}} \times \Lambda \mathbf{e} = \dot{\mathbf{w}} \times \mathbf{t} \quad (3.8)$$

Moreover, we can conclude from the above that the angular velocities $\dot{\boldsymbol{\psi}}$ and $\dot{\mathbf{w}}$ are constrained according to

$$\dot{\boldsymbol{\psi}} \cdot \mathbf{e} = 0; \quad \dot{\mathbf{w}} \cdot \mathbf{t} = 0 \Rightarrow \dot{\mathbf{w}} = \mathbf{t} \times \dot{\mathbf{t}} \quad (3.9)$$

An alternative possibility for constructing \mathbf{t}_t exploits the rotation vector with an additive update of the rotation parameters. By using the material rotation vector $\boldsymbol{\vartheta}$ we have³

$$\mathbf{t}_t = \tilde{\Lambda} (\boldsymbol{\vartheta} + t\dot{\boldsymbol{\vartheta}}) \mathbf{e} \quad (3.10)$$

³Eq. (3.10) defines rotation from \mathbf{e} to \mathbf{t}_t consequently including the initial rotation from \mathbf{e} to \mathbf{t}_0 . The material rotation vector $\boldsymbol{\vartheta}$ is thus having a non-zero initial value for any initially curved shell. This can be avoided by defining \mathbf{t}_t as

$$\mathbf{t}_t = \Lambda_0 \tilde{\Lambda} (\boldsymbol{\vartheta} + t\dot{\boldsymbol{\vartheta}}) \mathbf{e}$$

which sets the material rotation vector at the initial configuration to zero. The former approach is discussed in Ibrahimbegović Brank and Courtois [15], while the later is presented in Brank and Ibrahimbegović [7].

Time derivative of (3.10) gives

$$\dot{\mathbf{t}} = \mathbf{A}(\vartheta) \dot{\vartheta} \quad (3.11)$$

where

$$\mathbf{A}(\vartheta) = \left[-\frac{\sin \vartheta}{\vartheta} (\mathbf{e} \otimes \vartheta + \mathbf{E}) + \frac{\vartheta \cos \vartheta - \sin \vartheta}{\vartheta^3} (\vartheta \times \mathbf{e}) \otimes \vartheta \right] \quad (3.12)$$

and $\vartheta = \|\vartheta\|$, $\mathbf{E}\mathbf{b} = \mathbf{e} \times \mathbf{b}$. It also follows from (3.3) that

$$\dot{\vartheta} \cdot \mathbf{e} = 0 \quad (3.13)$$

Similar developments and constraints on rotation vector can be carried out in the spatial representation (see Brank, Mamouri and Ibrahimbegović [8] and Brank and Ibrahimbegović [7]) with the spatial rotation vector $\boldsymbol{\theta}$. The natural relationship of different velocity parameters can be expressed by the commutative diagram in Figure 2, where

$$\mathbf{B}(\vartheta) = \mathbf{E}\Lambda^T \mathbf{A}(\vartheta); \quad \mathbf{D}(\boldsymbol{\theta}) = \Lambda \mathbf{E}\Lambda^T \mathbf{A}(\vartheta) \quad (3.14)$$

In closing this section we turn to deriving expressions for the shell-director acceleration, where by taking time derivative of (3.8) and (3.11), we get (see Brank, Mamouri and Ibrahimbegović [8])

$$\ddot{\mathbf{t}} = \Lambda \left[-\mathbf{e}\dot{\psi}^2 + \ddot{\boldsymbol{\psi}} \times \mathbf{e} \right] \quad (3.15)$$

$$\ddot{\mathbf{t}} = -\mathbf{t}\dot{w}^2 + \ddot{\mathbf{w}} \times \mathbf{t} \quad (3.16)$$

where $\dot{\psi} = \|\dot{\boldsymbol{\psi}}\| = \dot{w} = \|\dot{\mathbf{w}}\|$ or yet

$$\ddot{\mathbf{t}} = \mathbf{Y}(\vartheta, \dot{\vartheta}) \dot{\vartheta} + \mathbf{A}(\vartheta) \ddot{\vartheta} \quad (3.17)$$

where $\mathbf{Y}(\vartheta, \dot{\vartheta})$ is given as

$$\begin{aligned} \mathbf{Y}(\vartheta, \dot{\vartheta}) &= -\frac{\sin \vartheta}{\vartheta} \mathbf{e} \otimes \dot{\vartheta} \\ &+ \frac{\vartheta \cos \vartheta - \sin \vartheta}{\vartheta^3} \left[-\vartheta \cdot \dot{\vartheta} (\mathbf{e} \otimes \vartheta + \mathbf{E}) + (\dot{\vartheta} \times \mathbf{e}) \otimes \vartheta + (\vartheta \times \mathbf{e}) \otimes \dot{\vartheta} \right] \\ &+ \frac{-\vartheta^2 \sin \vartheta - 3\vartheta \cos \vartheta + 3 \sin \vartheta}{\vartheta^5} (\vartheta \cdot \dot{\vartheta}) (\vartheta \times \mathbf{e}) \otimes \vartheta \end{aligned} \quad (3.18)$$

By making use of the relationship $\ddot{\mathbf{w}} = \Lambda \ddot{\boldsymbol{\psi}}$ (e.g. see Ibrahimbegović and Al Mikdad [14]) we can show that the following constraints hold

$$\ddot{\boldsymbol{\psi}} \cdot \mathbf{e} = 0; \quad \ddot{\mathbf{w}} \cdot \mathbf{t} = 0 \quad (3.19)$$

which can be supplemented with

$$\ddot{\boldsymbol{\vartheta}} \cdot \mathbf{e} = 0 \quad (3.20)$$

In the coordinate representation of the above introduced vectors and tensors one can exploit the constraints to obtain the reduced coordinate representation. Namely, the material rotational vectors can be presented by two components, while their spatial counterparts have to be expressed by three components which remain linearly dependent. Material and spatial vector-like objects associated with the rotation, velocity and acceleration of the shell-director vector are summarized in Table 1.

4. Implicit time integration schemes for shells with rotations

In the computational dynamics we partition the time interval of interest in a chosen number of time steps as $[t_0, T] = \bigcup_{n=0}^N [t_n, t_{n+1}]$. In order to avoid the singularity problems (see e.g. Ibrahimbegović, Brank and Courtois [15], Betsch, Menzel and Stein [3]), the total rotation vectors $\boldsymbol{\vartheta}$ and $\boldsymbol{\theta}$ introduced above can be replaced by the corresponding incremental rotation vectors $\boldsymbol{\vartheta}_{n+1}$ and $\boldsymbol{\theta}_{n+1}$ (e.g. see Ibrahimbegović [13]), which are reset to zero at the beginning of each time step. The rotation tensor at time t_{n+1} is then computed as

$$\begin{aligned} \Lambda_{n+1} &= \tilde{\Lambda}(\boldsymbol{\theta}_{n+1}) \Lambda_n \\ &= \Lambda_n \tilde{\Lambda}(\boldsymbol{\vartheta}_{n+1}) \end{aligned} \quad (4.1)$$

where

$$\boldsymbol{\theta}_{n+1} = \Lambda_n \boldsymbol{\vartheta}_{n+1} \quad (4.2)$$

which leads to two possibilities to define \mathbf{t}_{n+1} in terms of the incremental rotation vector

$$\mathbf{t}_{n+1} = \Lambda_n \tilde{\Lambda}(\boldsymbol{\vartheta}_{n+1}) \mathbf{e} = \tilde{\Lambda}(\boldsymbol{\theta}_{n+1}) \Lambda_n \mathbf{e} = \tilde{\Lambda}(\boldsymbol{\theta}_{n+1}) \mathbf{t}_n \quad (4.3)$$

By exploiting analogy with the total rotation vector we can conclude that the incremental rotation vectors $\boldsymbol{\vartheta}_{n+1}$ and $\boldsymbol{\theta}_{n+1}$ are subjected to the following constraints:

$$\boldsymbol{\vartheta}_{n+1} \cdot \mathbf{e} = 0; \quad \dot{\boldsymbol{\vartheta}}_{n+1} \cdot \mathbf{e} = 0; \quad \ddot{\boldsymbol{\vartheta}}_{n+1} \cdot \mathbf{e} = 0 \quad (4.4)$$

and (see Brank, Mamouri and Ibrahimbegović [8])

$$\begin{aligned} \boldsymbol{\theta}_{n+1} \cdot \mathbf{t}_{n+1} &= 0; \quad \dot{\boldsymbol{\theta}}_{n+1} \cdot \mathbf{t}_{n+1} = 0; \quad \boldsymbol{\theta}_{n+1} \cdot \dot{\mathbf{t}}_{n+1} = 0 \\ \ddot{\boldsymbol{\theta}}_{n+1} \cdot \mathbf{t}_{n+1} &= 0; \quad \dot{\boldsymbol{\theta}}_{n+1} \cdot \dot{\mathbf{t}}_{n+1} = 0, \quad \boldsymbol{\theta}_{n+1} \cdot \ddot{\mathbf{t}}_{n+1} = 0 \end{aligned} \quad (4.5)$$

Additional advantage of the incremental rotation vector is that it fits nicely with the time-stepping schemes, which we employed to obtain the evolution of the state variables for beams (Ibrahimbegović and Al Mikdad [14]) and shells (Brank, Mamouri and Ibrahimbegović [8]).

For a couple of one-step time-stepping schemes examined subsequently - the Newmark scheme and the energy conserving/decaying mid-point scheme - the central problem reduces to

$$\begin{aligned} \text{given : } & \varphi_n, \dot{\varphi}_n, \ddot{\varphi}_n \text{ and } \mathbf{t}_n, \dot{\mathbf{t}}_n, \ddot{\mathbf{t}}_n \\ \text{find : } & \varphi_{n+1}, \dot{\varphi}_{n+1}, \ddot{\varphi}_{n+1} \text{ and } \mathbf{t}_{n+1}, \dot{\mathbf{t}}_{n+1}, \ddot{\mathbf{t}}_{n+1} \end{aligned} \quad (4.6)$$

4.1. Newmark scheme

The Newmark family of algorithms (e.g. see Hughes [10], Bathe [1]) seeks to solve the central problem in (4.6) by imposing that the equations of motion are satisfied at the end of each considered step

$$\delta K_{n+1} + \delta \Pi_{n+1} = 0 \quad (4.7)$$

In order to make this problem well-posed we also need to provide the corresponding evolution of velocities and accelerations. In particular, for mid-surface displacement the standard implementation of the Newmark algorithm can be used to compute velocities and accelerations at time t_{n+1} with

$$\dot{\boldsymbol{\varphi}}_{n+1} = \frac{\gamma}{\beta \Delta t} \mathbf{u}_{n+1} + \frac{\beta - \gamma}{\beta} \dot{\boldsymbol{\varphi}}_n + \frac{(\beta - 0.5\gamma) \Delta t}{\beta} \ddot{\boldsymbol{\varphi}}_n \quad (4.8)$$

$$\ddot{\boldsymbol{\varphi}}_{n+1} = \frac{1}{\beta (\Delta t)^2} \mathbf{u}_{n+1} - \frac{1}{\beta \Delta t} \dot{\boldsymbol{\varphi}}_n - \frac{0.5 - \beta}{\beta} \ddot{\boldsymbol{\varphi}}_n \quad (4.9)$$

where $\mathbf{u}_{n+1} = \boldsymbol{\varphi}_{n+1} - \boldsymbol{\varphi}_n$ is incremental displacement, $\Delta t = t_{n+1} - t_n$, whereas β and γ are the Newmark parameters. Typical choice for $\beta = 1/4$ and $\gamma = 1/2$ leads to the scheme of second-order accuracy.

As noted by Simo and Vu-Quoc [22] and Ibrahimbegović and Al Mikdad [14] in their work on beams, the same kind of Newmark approximations for angular velocity and acceleration can directly be applied only in the material representation according to

$$\dot{\boldsymbol{\psi}}_{n+1} = \frac{\gamma}{\beta \Delta t} \boldsymbol{\vartheta}_{n+1} + \frac{\beta - \gamma}{\beta} \dot{\boldsymbol{\psi}}_n + \frac{(\beta - 0.5\gamma) \Delta t}{\beta} \ddot{\boldsymbol{\psi}}_n \quad (4.10)$$

$$\ddot{\boldsymbol{\psi}}_{n+1} = \frac{1}{\beta (\Delta t)^2} \boldsymbol{\vartheta}_{n+1} - \frac{1}{\beta \Delta t} \dot{\boldsymbol{\psi}}_n - \frac{0.5 - \beta}{\beta} \ddot{\boldsymbol{\psi}}_n \quad (4.11)$$

where $\boldsymbol{\vartheta}_{n+1}$ is the material incremental rotation vector which is zero at time t_n , while $\dot{\boldsymbol{\psi}}_n$ and $\ddot{\boldsymbol{\psi}}_n$ are the material shell director angular velocity and the material shell director angular acceleration at time t_n . The same approximations can be retained for smooth shells, since all vectors in (4.10) and (4.11) are constrained by lying in the tangent plane containing the vectors perpendicular to the fixed base vector \mathbf{e} , see (4.4). The shell-director velocity and acceleration follow from (3.8) and (3.15)

$$\dot{\mathbf{t}}_{n+1} = \Lambda_{n+1} \left(\dot{\boldsymbol{\psi}}_{n+1} \times \mathbf{e} \right); \quad \ddot{\mathbf{t}}_{n+1} = \Lambda_{n+1} \left(-\mathbf{e} \dot{\boldsymbol{\psi}}_{n+1}^2 + \ddot{\boldsymbol{\psi}}_{n+1} \times \mathbf{e} \right) \quad (4.12)$$

By inserting these Newmark approximations for velocities and accelerations into the weak form (4.7), we can obtain a system of non-linear algebraic equations with the incremental displacements \mathbf{u}_{n+1} and the incremental material rotation vector $\boldsymbol{\vartheta}_{n+1}$ as the unknowns. The central problem (4.6) can for this case be written as

$$\begin{aligned} \text{given : } & \boldsymbol{\varphi}_n, \dot{\boldsymbol{\varphi}}_n, \ddot{\boldsymbol{\varphi}}_n \text{ and } \mathbf{t}_n, \dot{\boldsymbol{\psi}}_n, \ddot{\boldsymbol{\psi}}_n \\ \text{find : } & \boldsymbol{\varphi}_{n+1}, \dot{\boldsymbol{\varphi}}_{n+1}, \ddot{\boldsymbol{\varphi}}_{n+1} \text{ and } \mathbf{t}_{n+1}, \dot{\mathbf{t}}_{n+1}, \ddot{\mathbf{t}}_{n+1} \text{ satisfying (4.7)} \end{aligned} \quad (4.13)$$

One can also obtain the spatial form of the Newmark approximations for angular velocities and accelerations (see Ibrahimbegović and Al Mikdad [14], Brank, Mamouri and Ibrahimbegović [8]) according to

$$\dot{\mathbf{w}}_{n+1} = \Lambda(\boldsymbol{\theta}_{n+1}) \left[\frac{\gamma}{\beta \Delta t} \boldsymbol{\theta}_{n+1} + \frac{\beta - \gamma}{\beta} \dot{\mathbf{w}}_n + \frac{(\beta - 0.5\gamma) \Delta t}{\beta} \ddot{\mathbf{w}}_n \right] \quad (4.14)$$

$$\ddot{\mathbf{w}}_{n+1} = \Lambda(\boldsymbol{\theta}_{n+1}) \left[\frac{1}{\beta (\Delta t)^2} \boldsymbol{\theta}_{n+1} - \frac{1}{\beta \Delta t} \dot{\mathbf{w}}_n - \frac{0.5 - \beta}{\beta} \ddot{\mathbf{w}}_n \right] \quad (4.15)$$

where $\boldsymbol{\theta}_{n+1}$ is the spatial incremental rotation vector which is zero at time t_n , while $\dot{\mathbf{w}}_n$ and $\ddot{\mathbf{w}}_n$ are the spatial angular velocity and the spatial angular acceleration at time t_n . Shell-director velocity and acceleration follow from (3.8) and (3.16) as

$$\dot{\mathbf{t}}_{n+1} = \dot{\mathbf{w}}_{n+1} \times \mathbf{t}_{n+1}; \quad \ddot{\mathbf{t}}_{n+1} = \ddot{\mathbf{w}}_{n+1} \times \mathbf{t}_{n+1} - \mathbf{t}_{n+1} \dot{w}_{n+1}^2 \quad (4.16)$$

By replacing the spatial form of the Newmark approximations into the weak form of the momentum balance equation (4.7) we obtain a system of non-linear equations in the incremental displacements \mathbf{u}_{n+1} and the incremental spatial rotation vector $\boldsymbol{\theta}_{n+1}$ as the unknowns. The central problem (4.6) transforms to

$$\text{given : } \varphi_n, \dot{\varphi}_n, \ddot{\varphi}_n \text{ and } \mathbf{t}_n, \dot{\mathbf{w}}_n, \ddot{\mathbf{w}}_n \quad (4.17)$$

$$\text{find : } \varphi_{n+1}, \dot{\varphi}_{n+1}, \ddot{\varphi}_{n+1} \text{ and } \mathbf{t}_{n+1}, \dot{\mathbf{t}}_{n+1}, \ddot{\mathbf{t}}_{n+1} \text{ satisfying (4.7)}$$

Yet another possibility to obtain the shell-director velocity and acceleration at time t_{n+1} is to use the Newmark approximations directly in terms of the shell-director vector time derivatives as

$$\dot{\mathbf{t}}_{n+1} = \frac{\gamma}{\beta \Delta t} (\mathbf{t}_{n+1} - \mathbf{t}_n) + \frac{\beta - \gamma}{\beta} \dot{\mathbf{t}}_n + \frac{\beta - 0.5\gamma}{\beta} \Delta t \ddot{\mathbf{t}}_n \quad (4.18)$$

$$\ddot{\mathbf{t}}_{n+1} = \frac{1}{\beta (\Delta t)^2} (\mathbf{t}_{n+1} - \mathbf{t}_n) - \frac{1}{\beta \Delta t} \dot{\mathbf{t}}_n - \frac{0.5 - \beta}{\beta} \ddot{\mathbf{t}}_n \quad (4.19)$$

Approximations (4.18) and (4.19) can be desirable to use for simplicity despite the fact that such a version does not have a clear geometric representation.

Detailed presentation of the corresponding linearization form of the momentum balance equation for Newmark scheme is given in Brank, Mamouri and Ibrahimbegović [8].

4.2. Energy conserving/decaying mid-point scheme

The standard mid-point scheme would seek to solve the central problem in (4.6) by imposing that the momentum balance equations of shell are satisfied at time $t_{n+1/2} = \frac{1}{2}(t_n + t_{n+1})$, which is denoted as

$$\delta K_{n+1/2} + \delta \Pi_{n+1/2} = 0 \quad (4.20)$$

where

$$\begin{aligned}
\delta K_{n+1/2} &= \int_A \left(\delta \boldsymbol{\varphi} \cdot A_\rho \ddot{\boldsymbol{\varphi}}_{n+1/2} + \delta \mathbf{t} \cdot I_\rho \ddot{\mathbf{t}}_{n+1/2} \right) dA \\
&= \int_A \left(\delta \boldsymbol{\varphi} \cdot \dot{\mathbf{p}}_{n+1/2} + \delta \mathbf{t} \cdot \dot{\boldsymbol{\pi}}_{n+1/2} \right) dA \\
&= \frac{1}{\Delta t} \int_A \left[\delta \boldsymbol{\varphi} \cdot (\mathbf{p}_{n+1} - \mathbf{p}_n) + \delta \mathbf{t} \cdot (\boldsymbol{\pi}_{n+1} - \boldsymbol{\pi}_n) \right] dA
\end{aligned} \tag{4.21}$$

In (4.20) and (4.21) above

$$\mathbf{p} = A_\rho \dot{\boldsymbol{\varphi}} \text{ and } \boldsymbol{\pi} = I_\rho \dot{\mathbf{t}} \tag{4.22}$$

denote, respectively, the linear and the angular momenta of the shell, whereas

$$\delta \Pi_{n+1/2} = \int_A \left[n_{n+1/2}^{\alpha\beta} \delta \varepsilon_{\alpha\beta} + q_{n+1/2}^\alpha \delta \gamma_\alpha + m_{n+1/2}^{\alpha\beta} \delta \kappa_{\alpha\beta} \right] dA - \delta \Pi_{ext, n+1/2} \tag{4.23}$$

where $\delta \varepsilon_{\alpha\beta}$, $\delta \gamma_\alpha$ and $\delta \kappa_{\alpha\beta}$ are variations of the strain measures of the shell configuration at the middle of the time step, which is defined as

$$\boldsymbol{\varphi}_{n+1/2} = \frac{1}{2} (\boldsymbol{\varphi}_n + \boldsymbol{\varphi}_{n+1}); \quad \mathbf{t}_{n+1/2} = \frac{1}{2} (\mathbf{t}_n + \mathbf{t}_{n+1}) \tag{4.24}$$

No accelerations appear in the final form of $\delta K_{n+1/2}$. It is important to note that the shell-director variation $\delta \mathbf{t}$ has to satisfy constraint condition $\mathbf{t}_{n+1/2} \cdot \delta \mathbf{t} = 0$. The linear and the angular momenta in (4.21) can be obtained from the mid-point approximation of the corresponding evolution equations according to

$$\begin{aligned}
\boldsymbol{\varphi}_{n+1} - \boldsymbol{\varphi}_n &= \frac{\Delta t}{2} (\dot{\boldsymbol{\varphi}}_n + \dot{\boldsymbol{\varphi}}_{n+1}) = \frac{\Delta t}{2A_\rho} (\mathbf{p}_n + \mathbf{p}_{n+1}) = \frac{\Delta t}{A_\rho} \mathbf{p}_{n+1/2} \Rightarrow \\
\dot{\boldsymbol{\varphi}}_{n+1} &= \frac{2}{\Delta t} (\boldsymbol{\varphi}_{n+1} - \boldsymbol{\varphi}_n) - \dot{\boldsymbol{\varphi}}_n
\end{aligned} \tag{4.25}$$

for the displacement and

$$\begin{aligned}
\mathbf{t}_{n+1} - \mathbf{t}_n &= \frac{\Delta t}{2} (\dot{\mathbf{t}}_n + \dot{\mathbf{t}}_{n+1}) = \frac{\Delta t}{2I_\rho} (\boldsymbol{\pi}_n + \boldsymbol{\pi}_{n+1}) = \frac{\Delta t}{I_\rho} \boldsymbol{\pi}_{n+1/2} \Rightarrow \\
\dot{\mathbf{t}}_{n+1} &= \frac{2}{\Delta t} (\mathbf{t}_{n+1} - \mathbf{t}_n) - \dot{\mathbf{t}}_n
\end{aligned} \tag{4.26}$$

for the shell director rotation. With the above approximations the central problem in (4.6) transforms to

$$\begin{aligned}
\text{given : } & \boldsymbol{\varphi}_n, \dot{\boldsymbol{\varphi}}_n \text{ and } \mathbf{t}_n, \dot{\mathbf{t}}_n \\
\text{find : } & \boldsymbol{\varphi}_{n+1}, \dot{\boldsymbol{\varphi}}_{n+1} \text{ and } \mathbf{t}_{n+1}, \dot{\mathbf{t}}_{n+1} \text{ satisfying (4.20)}
\end{aligned} \tag{4.27}$$

Accelerations $\ddot{\varphi}_{n+1}$ and $\ddot{\mathbf{t}}_{n+1}$ are obtained from post-processing as

$$\begin{aligned}
\dot{\varphi}_{n+1} - \dot{\varphi}_n &= \frac{\Delta t}{2} (\ddot{\varphi}_n + \ddot{\varphi}_{n+1}) \Rightarrow \\
\ddot{\varphi}_{n+1} &= \frac{2}{\Delta t} (\dot{\varphi}_{n+1} - \dot{\varphi}_n) - \ddot{\varphi}_n = \frac{4}{(\Delta t)^2} (\varphi_{n+1} - \varphi_n) - \frac{4}{\Delta t} \dot{\varphi}_n - \ddot{\varphi}_n \\
\dot{\mathbf{t}}_{n+1} - \dot{\mathbf{t}}_n &= \frac{\Delta t}{2} (\ddot{\mathbf{t}}_n + \ddot{\mathbf{t}}_{n+1}) \Rightarrow \\
\ddot{\mathbf{t}}_{n+1} &= \frac{2}{\Delta t} (\dot{\mathbf{t}}_{n+1} - \dot{\mathbf{t}}_n) - \ddot{\mathbf{t}}_n = \frac{4}{(\Delta t)^2} (\mathbf{t}_{n+1} - \mathbf{t}_n) - \frac{4}{\Delta t} \dot{\mathbf{t}}_n - \ddot{\mathbf{t}}_n
\end{aligned} \tag{4.28}$$

It turns out that mid-point approximations (4.25), (4.26) and (4.28) can be obtained by setting $\gamma/\beta = 2$ and $\beta = 1/4$ in Newmark formulas (4.8), (4.9), (4.18) and (4.19).

We note that the mid-point approximation in (4.25) and (4.26) above can be employed to express the kinetic energy variation as the difference of the corresponding values at the ends of the step. Namely, by choosing the virtual displacements and rotations as $\delta\varphi = \varphi_{n+1} - \varphi_n$, $\delta\mathbf{t} = \mathbf{t}_{n+1} - \mathbf{t}_n$ we obtain from (4.21), (4.25) and (4.26) that

$$\begin{aligned}
\delta K_{n+1/2} &= \frac{1}{2} \int_A \left[\frac{1}{A_\rho} \mathbf{p}_{n+1} \cdot \mathbf{p}_{n+1} + \frac{1}{I_\rho} \boldsymbol{\pi}_{n+1} \cdot \boldsymbol{\pi}_{n+1} - \frac{1}{A_\rho} \mathbf{p}_n \cdot \mathbf{p}_n - \frac{1}{I_\rho} \boldsymbol{\pi}_n \cdot \boldsymbol{\pi}_n \right] dA \\
&= K(\varphi_{n+1}, \mathbf{t}_{n+1}) - K(\varphi_n, \mathbf{t}_n)
\end{aligned} \tag{4.29}$$

We note in passing that the choice we made for variation of the director vector satisfies the constraint condition in the middle of the time step with

$$\mathbf{t}_{n+1/2} \cdot \delta\mathbf{t} = \frac{1}{2} (\mathbf{t}_n + \mathbf{t}_{n+1}) \cdot (\mathbf{t}_{n+1} - \mathbf{t}_n) = 0 \Rightarrow \mathbf{t}_{n+1} \cdot \mathbf{t}_{n+1} = \mathbf{t}_n \cdot \mathbf{t}_n \tag{4.30}$$

The same choice of virtual displacements and rotations allows us to express the virtual strain measures as the corresponding difference of the real strain measures at the end of the time step, since with respect to (2.6) we can write

$$\begin{aligned}
\delta\varepsilon_{\alpha\beta} &= \frac{1}{2} \left(\delta\varphi_{,\alpha} \cdot \varphi_{n+1/2,\beta} + \varphi_{n+1/2,\alpha} \cdot \delta\varphi_{,\beta} \right) \\
&= \frac{1}{2} (\varphi_{n+1,\alpha} \cdot \varphi_{n+1,\beta} - \varphi_{n,\alpha} \cdot \varphi_{n,\beta}) \\
&= \varepsilon_{\alpha\beta,n+1} - \varepsilon_{\alpha\beta,n}
\end{aligned} \tag{4.31}$$

and

$$\begin{aligned}
\delta\gamma_\alpha &= \delta\varphi_{,\alpha} \cdot \mathbf{t}_{n+1/2} + \varphi_{n+1/2,\alpha} \cdot \delta\mathbf{t} \\
&= \varphi_{n+1,\alpha} \cdot \mathbf{t}_{n+1,\beta} - \varphi_{n,\alpha} \cdot \mathbf{t}_{n,\beta} \\
&= \gamma_{\alpha,n+1} - \gamma_{\alpha,n}
\end{aligned} \tag{4.32}$$

Similarly, in accordance with (2.8) we can obtain that

$$\begin{aligned}
\delta\kappa_{\alpha\beta} &= \delta\varphi_{,\alpha} \cdot \mathbf{t}_{n+1/2,\beta} + \varphi_{n+1/2,\alpha} \cdot \delta\mathbf{t}_{,\beta} \\
&= \varphi_{n+1,\alpha} \cdot \mathbf{t}_{n+1,\beta} - \varphi_{n,\alpha} \cdot \mathbf{t}_{n,\beta} \\
&= \kappa_{\alpha\beta,n+1} - \kappa_{\alpha\beta,n}
\end{aligned} \tag{4.33}$$

The interpretation of the constitutive equations (2.11) in (4.23) is now made in an algorithmic sense (see Simo and Tarnow [24]) with

$$n_{n+1/2}^{\alpha\beta} \rightarrow n^{\alpha\beta} = \frac{Eh}{1-\nu^2} H^{\alpha\beta\gamma\delta} \frac{1}{2} [\varepsilon_{\gamma\delta,n+1} + \varepsilon_{\gamma\delta,n}] \quad (4.34)$$

$$q_{n+1/2}^{\alpha} \rightarrow q^{\alpha} = \varkappa Ghg^{\alpha\beta} \frac{1}{2} [\gamma_{\beta,n+1} + \gamma_{\beta,n}] \quad (4.35)$$

and

$$m_{n+1/2}^{\alpha\beta} \rightarrow m^{\alpha\beta} = \frac{Eh^3}{12(1-\nu^2)} H^{\alpha\beta\gamma\delta} \frac{1}{2} [\kappa_{\gamma\delta,n+1} + \kappa_{\gamma\delta,n}] \quad (4.36)$$

which allows us to express the internal energy variation in (4.23) as

$$\begin{aligned} \delta\Pi_{n+1/2} &= \frac{1}{2} \int_A \left[n_{n+1}^{\alpha\beta} \varepsilon_{\alpha\beta,n+1} + q_{n+1}^{\alpha} \gamma_{\alpha,n+1} + m_{n+1}^{\alpha\beta} \kappa_{\alpha\beta,n+1} \right. \\ &\quad \left. - n_n^{\alpha\beta} \varepsilon_{\alpha\beta,n} - q_n^{\alpha} \gamma_{\alpha,n} - m_n^{\alpha\beta} \kappa_{\alpha\beta,n} \right] dA \\ &= \Pi(\boldsymbol{\varphi}_{n+1}, \mathbf{t}_{n+1}) - \Pi(\boldsymbol{\varphi}_n, \mathbf{t}_n) \end{aligned} \quad (4.37)$$

With the results in (4.29) and (4.37) we can see that the above algorithm is designed so that the total energy remains preserved in any free vibration phase.

An alternative modification of the mid-point scheme to the one given in (4.25) and (4.26) - which conserves the total energy - is the scheme described subsequently which is capable of assuring that the total energy is always dissipated. To that end we can modify the algorithmic constitutive equations in (4.34) to (4.36) in order to include the dissipating term according to

$$n^{\alpha\beta} = \frac{Eh}{1-\nu^2} H^{\alpha\beta\gamma\delta} \left[\frac{1}{2} (\varepsilon_{\gamma\delta,n+1} + \varepsilon_{\gamma\delta,n}) + \tilde{\alpha} (\varepsilon_{\gamma\delta,n+1} - \varepsilon_{\gamma\delta,n}) \right] \quad (4.38)$$

$$q^{\alpha} = \varkappa Ghg^{\alpha\beta} \left[\frac{1}{2} (\gamma_{\beta,n+1} + \gamma_{\beta,n}) + \tilde{\alpha} (\gamma_{\beta,n+1} - \gamma_{\beta,n}) \right] \quad (4.39)$$

and

$$m^{\alpha\beta} = \frac{Eh^3}{12(1-\nu^2)} H^{\alpha\beta\gamma\delta} \left[\frac{1}{2} (\kappa_{\gamma\delta,n+1} + \kappa_{\gamma\delta,n}) + \tilde{\alpha} (\kappa_{\gamma\delta,n+1} - \kappa_{\gamma\delta,n}) \right] \quad (4.40)$$

where $\tilde{\alpha} \in [0, 1]$ is the chosen coefficient which controls the potential energy dissipation $D_M \geq 0$, as can easily be seen from expressing the variation in (4.20) as

$$\delta\Pi_{n+1/2} = \Pi(\boldsymbol{\varphi}_{n+1}, \mathbf{t}_{n+1}) - \Pi(\boldsymbol{\varphi}_n, \mathbf{t}_n) + D_M \quad (4.41)$$

where

$$\begin{aligned} D_M &= \tilde{\alpha} \int_A \left[(\varepsilon_{\alpha\beta,n+1} - \varepsilon_{\alpha\beta,n}) \frac{Eh}{1-\nu^2} H^{\alpha\beta\gamma\delta} (\varepsilon_{\gamma\delta,n+1} - \varepsilon_{\gamma\delta,n}) \right. \\ &\quad \left. + (\gamma_{\alpha,n+1} - \gamma_{\alpha,n}) \varkappa Ghg^{\alpha\beta} (\gamma_{\beta,n+1} - \gamma_{\beta,n}) \right. \\ &\quad \left. + (\kappa_{\alpha\beta,n+1} - \kappa_{\alpha\beta,n}) \frac{Eh^3}{12(1-\nu^2)} H^{\alpha\beta\gamma\delta} (\kappa_{\gamma\delta,n+1} - \kappa_{\gamma\delta,n}) \right] dA \end{aligned} \quad (4.42)$$

It is also interesting to note that the proposed modifications of algorithmic constitutive equations in (4.38) to (4.40) differs significantly from the energy conserving counterparts in (4.34) to (4.36) mostly for high frequency modes where the numerical values of strains at the ends of the time interval can be quite apart. The dissipation is thus introduced mainly for these higher modes, which reduces their contribution and proves helpful for stability of the computation. Similar modification is introduced for the evolution equation in (4.25) and (4.26) used for energy-conserving scheme, leading to

$$\begin{aligned}\varphi_{n+1} - \varphi_n &= \frac{\Delta t}{2} (\dot{\varphi}_n + \dot{\varphi}_{n+1}) + \tilde{\beta} \Delta t (\dot{\varphi}_{n+1} - \dot{\varphi}_n) \Rightarrow \\ \dot{\varphi}_{n+1} &= \frac{1}{(\Delta t/2 + \tilde{\beta} \Delta t)} \left[\varphi_{n+1} - \varphi_n - \dot{\varphi}_n \left(\frac{\Delta t}{2} - \tilde{\beta} \Delta t \right) \right]\end{aligned}\quad (4.43)$$

and

$$\begin{aligned}\mathbf{t}_{n+1} - \mathbf{t}_n &= \frac{\Delta t}{2} (\dot{\mathbf{t}}_n + \dot{\mathbf{t}}_{n+1}) + \tilde{\beta} \Delta t (\dot{\mathbf{t}}_{n+1} - \dot{\mathbf{t}}_n) \Rightarrow \\ \dot{\mathbf{t}}_{n+1} &= \frac{1}{(\Delta t/2 + \tilde{\beta} \Delta t)} \left[\mathbf{t}_{n+1} - \mathbf{t}_n - \dot{\mathbf{t}}_n \left(\frac{\Delta t}{2} - \tilde{\beta} \Delta t \right) \right]\end{aligned}\quad (4.44)$$

With these approximations on hand the variation of kinetic energy in (4.21) reduces to

$$\delta K_{n+1/2} = K_{n+1} - K_n + D_K; \quad D_K \geq 0 \quad (4.45)$$

where

$$D_K = \tilde{\beta} \int_A [(\dot{\varphi}_{n+1} - \dot{\varphi}_n) A_\rho (\dot{\varphi}_{n+1} - \dot{\varphi}_n) + (\dot{\mathbf{t}}_{n+1} - \dot{\mathbf{t}}_n) I_\rho (\dot{\mathbf{t}}_{n+1} - \dot{\mathbf{t}}_n)] dA \quad (4.46)$$

which shows that parameter $\tilde{\beta} \in [0, 1]$ can be used to control the introduced dissipation in the kinetic energy term.

5. Numerical examples

In this section we present results obtained in numerical simulations. The computations with the Newmark time stepping scheme were carried out by a research version of the computer program FEAP, developed by Prof. R. L. Taylor at UC Berkeley (see Zienkiewicz and Taylor [25]). The computations with the energy conserving/decaying scheme were carried out by a research version of the computer program AceGen (see Korelc [16], [17]).

A four-noded isoparametric shell finite element with assumed strain interpolations for transverse strains (see e.g. Brank, Perić and Damjanić [5]) was used to that end with either the incremental material rotation vector or the total rotation vector chosen for the parametrization of the shell-director motion (see Table 2). Numerical 2-point Gauss through-the-thickness integration was performed (although variation of metrics along the ζ coordinate was not taken into account) for the finite element used with the energy conserving (EC) and the energy decaying

(ED) schemes, while the finite element formulation with the Newmark (N) scheme employed an analytical through-the-thickness integration.

Two forms of the Newmark approximations (with $\beta = 1/4$ and $\gamma = 1/2$) for the shell-director velocity and acceleration were examined (see Table 2). As shown in the previous section, the EC and the ED schemes were both constructed directly in terms of the shell-director vector time derivatives which correspond to "version 2" of the Newmark scheme. The convergence tolerance of 10^{-9} for the norm of the residual vector was used in all examples.

In all figures X, Y, Z and tX, tY, tZ define the mid-surface and the shell director-vector quantities, respectively, in directions defined by the coordinate axes.

Example 1: Motion of a short cylinder This example was considered by Simo and Tarnow [24] and Brank, Briseghella, Tonello and Damjanić [6] to show the stability of the EC scheme for long-term computations. We note that the rotation parameters used in those two works, which were $\dot{\psi} \times \mathbf{e}$, are different of the rotation parameters employed in the present work (see Brank and Ibrahimbegović [7] for the relationships between different finite rotation parametrizations).

Geometry of the short cylinder is defined with radius $R = 7.5$, height $H = 3$ and thickness $h = 0.02$. The material characteristics are: Young's modulus $E = 2 \times 10^8$, Poisson's ratio $\nu = 0.5$ and mass density $\rho = 1$. The mid-surface mass density and the inertia term with respect to the mid-surface are $A_\rho = h\rho = 0.02$ and $I_\rho = \frac{\rho h^3}{12} = 6.667 \times 10^{-7}$, respectively. Displacements, rotations, velocities and accelerations at the initial time $t = 0$ are all zero. The loading conditions are presented in Figure 3 and Table 3. The response of the shell, meshed by 28×3 elements, is calculated with $\Delta t = 0.05$ for the Newmark scheme, and with initial $\Delta t = 0.1$ for the EC and the ED schemes.

Results are presented for "version 1" of the Newmark scheme, the EC scheme and the ED scheme with $\tilde{\alpha} = \tilde{\beta} = 0.2$ (in figures denoted as N, EC and 0.2, respectively). When the loads are removed (at time $t = 1$) the structure exhibits complex free motion in the 3d space. Evolutions of displacements and velocities of a point, which is initially located at $(R, 0, 0)$, are presented in Figures 4, 5 and 6 for $t \in [0, 5.5]$. It can be observed that the displacement curves of the Newmark scheme are practically identical to the EC solutions (Fig 4), and that the Newmark and the EC mid-surface velocity curves differ only slightly (Fig 5) from each other. On the other hand, a sharp difference in smoothness can be observed between the EC and the ED results shown in Figures 5 and 6. This is specially true for the shell-director velocities in the direction of X and Y coordinates (Fig. 6). It can be also observed from the displacement and the velocity curves that the ED scheme produces phase shift effect. This effect is due to the introduction of damping parameter $\tilde{\beta}$ in the evolution equations for velocities. In general, the bigger the ratio between the kinetic and the potential energy is, the more significant phase shift is expected if the same numerical value is used for both $\tilde{\alpha}$ and $\tilde{\beta}$ parameters. Figure 7 shows that the ration between the kinetic and the potential energy is for the present case approximately $5 : 1$, which leads to a considerable phase shift. We can therefore conclude for this example that the ED scheme, with relatively high introduced energy dissipation ($\tilde{\alpha} = \tilde{\beta} = 0.2$), smooths velocity curves, yet at the some time produces phase shift in displacements and velocities, so that the ED results eventually differ relatively significantly from the Newmark and the EC solutions. Energy curves are presented in Figure 7. It can be seen that the EC scheme conserves the total energy of the shell when the forces are removed. It can be also seen that relatively big energy dissipation is introduced for the chosen value of dissipation parameters $\tilde{\alpha} = \tilde{\beta} = 0.2$.

Although not shown in Figures, the present EC solutions are identical to those reported by Brank, Briseghella, Tonello and Damjanić [6], and are very close to those of Simo and Tarnow [24] (see [6] for further comments). This numerically confirms theoretical conclusions (see Brank and Ibrahimbegović [7]) that a choice of the rotational parameters has no influence on the results in the domain where specific parametrization is to provide solution.

Example 2: Dynamic buckling of a spherical cup The geometry and the material characteristics of one half of a sphere with a top hole are defined in Figure 8. The shell is meshed into 32×8 finite elements. Vertical displacements (in Z direction) are set to zero at the nodes of the bottom ring. Force $f(t) = 1.5p(t)$, where $p(t)$ is defined in Figure 8, is applied at each node of the top ring in the $-Z$ direction. The time step for the Newmark scheme is $\Delta t = 0.01$ and the initial time step for the EC and the ED scheme is $\Delta t = 0.1$.

Two different Newmark schemes are used to compute this example, referred as "version 1" and "version 2" in Table 2. Figure 9 shows vertical displacement of a node initially located at $A = (R \sin \alpha_1, 0, R \cos \alpha_1)$ for both versions. It can be seen that they produce identical results up to approximately $t = 4$, when the scheme which interpolates the time derivatives of the shell-director vector ("version 2") diverges for the chosen time step. This can lead to the conclusion that the scheme which interpolates the angular velocities and accelerations ("version 1") allows for bigger time steps.

The EC and the ED predictions (for $\tilde{\alpha} = \tilde{\beta} = 0.01$; $\tilde{\alpha} = \tilde{\beta} = 0.1$; $\tilde{\alpha} = \tilde{\beta} = 0.2$) of the displacements, the middle-surface velocities and the shell-director velocities of point A are presented in Figures 10, 11 and 12, respectively. Again the introduced dissipation smooths considerably displacement and velocity curves even for the smallest introduced dissipation ($\tilde{\alpha} = \tilde{\beta} = 0.01$). Figs. 10 and 11 show that the amount of a phase shift relates directly to the value of dissipation parameters. The time evolution of the kinetic, the potential and the total energy is further presented in Figures 13, 14 and 15, respectively. It can be observed that even the smallest introduced energy dissipation produces considerable dissipation of the total energy at the final calculation time $t = 10$. Figure 16 further shows time dependency of the vertical reaction force at node A . Again, the introduced dissipation smooths the response curve.

Figure 17 presents the size of the time step Δt , which is needed for the convergence to occur between 4 and 11 iterations. If the convergence is not reached within this number of iterations, the time step size is either doubled or reduced by one half. It can be seen that if more dissipation is induced, the larger the time step can be, which can lead to the conclusion that the controlled energy dissipation is numerically desirable. A sequence of deformed configurations is compared in Figure 18.

Example 3: Dynamic buckling of an ellipsoidal cup This example was considered by Brank, Briseghella, Tonello and Damjanić [6] and it is similar to the Example 2, except that the shell is more shallow and that its mass density is much smaller. The geometry, the material characteristics and the loading for this problem are given in Figure 19. The initial shell mid-surface is defined in spherical coordinates as $X = R \cos \theta \cos \varphi$, $Y = R \cos \theta \sin \varphi$, $Z = \frac{1}{2} R \cos \theta$, where $\theta \in [\arcsin(R_{\min}/R_{\max}), \pi/2]$, $\varphi \in [0, 2\pi]$ and $R = R_{\max}$. The initial shell normal of point with coordinates X, Y, Z is in the direction given by $X/2, Y/2, 2Z$. The shell is discretised by 32×8 finite elements with vertical nodal displacements at $Z = 0$ set to zero. Response is calculated with the EC and the ED schemes with the initial time step $\Delta t = 0.05$.

Figure 20 shows evolution of X and Z displacements of a node with the initial position $B = (R_{\min}, 0, H)$. Very similar responses are obtained both with the EC and the ED scheme (with $\tilde{\alpha} = \tilde{\beta} = 0.1$ and $\tilde{\alpha} = \tilde{\beta} = 0.2$). However, the EC scheme shows short-wave oscillations, which are damped if the ED scheme is used. Figure 21 shows the bigger rotation component of the shell-director vector initially located at B . Large oscillations can be observed again from the EC solutions, which are smoothed when energy dissipation is introduced. Time history of energies is given in Figures 22, 23 and 24. We note that the kinetic energy is negligible up to the snap-through (Fig. 22) and that the ED scheme dissipates all the kinetic energy immediately (both for $\tilde{\alpha} = \tilde{\beta} = 0.1$ and $\tilde{\alpha} = \tilde{\beta} = 0.2$) after new stable configuration is reached. On the other hand the EC scheme predicts infinite small vibrations, never setting them to zero. For the configurations following the snap-through a considerable difference between the EC and the ED predictions (both for $\tilde{\alpha} = \tilde{\beta} = 0.1$ and $\tilde{\alpha} = \tilde{\beta} = 0.2$) of the total energy is evident (Fig. 24). A sequence of deformed configurations in Figure 26 shows that the EC scheme predicts non symmetric vibrations towards the end of the buckling process, which may be more realistic than the ED scheme results predicting very smooth symmetric deformations. From the above we may conclude that the dissipation parameters used in this case are too big.

Figure 25 presents the size of the time step Δt , which is needed for the convergence to occur between 4 and 11 iterations for the ED scheme and between 4 to 15 iterations for the EC scheme. A consequence of undamped vibrations is very small Δt , which causes problems getting results for a long-term response. For this reason the results of the EC scheme are calculated and presented only to approximately $t = 1.8$.

Although not shown in figures the present EC solutions are very close to those reported by Brank, Briseghella, Tonello and Damjanić [6], where the response was calculated up to $t = 4.5$ with $\Delta t = 0.0015$.

6. Conclusions

In this work we elaborated upon the time-stepping schemes for nonlinear dynamics of smooth shells. The first issue which was clarified pertains the choice of the finite rotation parameters for the shell model of this kind, with the commutative diagram of the shell director velocity presenting relations among all the different representations. The latter proved to be of great interest for constructing three different versions of the Newmark time stepping scheme, and identifying the one employing the material representation of the incremental rotation vector as the most suitable for smooth shells.

The second type of time-stepping scheme for nonlinear dynamics of elastic shells, the mid-point rule, is explored herein in two different variants capable of ensuring either energy conserving or energy decaying computed response. The latter is proved to be particularly useful for damping out high frequency modes and thus assuring the stability of the computed response and more smooth time history of displacements, velocities and stress resultant components. However, one has to carefully choose the values of the introduced damping parameters.

Acknowledgment This work was supported by the Ministry of Education, Science and Sport of Slovenia, and by the French Ministry of Research and Education.

References

- [1] Bathe K.J. (1996): Finite Element Procedures, Prentice Hall, Englewood Cliffs, New York.
- [2] Bathe K.J. and Dvorkin E. (1985): A Four-Node Plate Bending Element Based on Mindlin/Reissner Plate Theory and Mixed Interpolation, *Int. J. Numer. Methods Eng.*, 21, 367-383.
- [3] Betsch, P.; Menzel, A.; Stein, E. (1998): On the parametrization of finite rotations in computational mechanics. A classification of concepts with application to smooth shells. *Comput. Methods Appl. Mech. Engrg.*, 155, 273-305.
- [4] Bottaso, C.L., Bauchau, O.A, Choi, J.-Y. (2002): An energy decaying scheme for nonlinear dynamics of shells, *Comput. Methods Appl. Mech. Engrg.*
- [5] Brank, B.; Perić, D.; Damjanić, F.B. (1995): On implementation of a non-linear four-node shell finite element for thin multilayered elastic shells. *Comp. Mech.*, 16, 341-359.
- [6] Brank, B.; Briseghella, L.; Tonello, N.; Damjanić, F.B. (1998): On non-linear dynamics of shells: Implementation of energy-momentum conserving algorithm for a finite rotation shell model. *Int. J. Numer. Meth. Engng.*, 42, 409-442.
- [7] Brank, B.; Ibrahimbegović, A. (2001): On the relation between different parametrizations of finite rotations for shells. *Eng. Comput.* 18, 950-973.
- [8] Brank, B. Mamouri S. and Ibrahimbegovic A. (2002): Constrained Finite Rotations in Dynamics of Shells and Newmark Implicit Time-Stepping Schemes, *Computer Modelling in Engineering and Science* (in press).
- [9] Hughes, T. J. R., Pister, K. S. (1978): Consistent linearization in mechanics of solids and structures, *Computers and Structures*, 8, 391-397.
- [10] Hughes, T. J. R. (1987): Finite Element Method: Linear Static and Dynamic Analysis, Prentice-Hall.
- [11] Ibrahimbegović, A.; Frey, F; Kožar I. (1995): Computational aspects of vector-like parametrization of three-dimensional finite rotations. *Int. J. Numer. Meth. Engng.*, 38, 3653-3673.
- [12] Ibrahimbegović, A. (1997): Stress resultant geometrically exact shell theory for finite rotations and its fe implementation. *ASME Appl. Mech. Review*, 50, 199-226.
- [13] Ibrahimbegović, A. (1997): On the Choice of Finite Rotation Parameters, *Comp. Methods Appl. Mech. Eng.*, 149, 49-71.
- [14] Ibrahimbegović, A.; Al Mikdad, M. (1998): Finite rotations in dynamics of beams and implicit time-stepping schemes. *Int. J. Numer. Meth. Engng.*, 41, 781-814.
- [15] Ibrahimbegović, A.; Brank, B.; Courtois, P. (2001): Stress resultant geometrically exact form of classical shell model and vector-like parametrization of constrained finite rotations. *Int. J. Numer. Meth. Engng.*, 52, 1235-1252.

- [16] Korelc, J. (2001): Automatic generation of numerical codes with introduction to AceGen 4.0 symbolic code generator, University of Ljubljana, Faculty of Civil and Geodetic Engineering, www.fgg.uni-lj.si/Symech/.
- [17] Korelc, J. (1997): Automatic generation of finite element code by simultaneous optimization of expressions, *Theor. Comput. Sci.*, 187, 231-248 (1997).
- [18] D. Kuhl, E. Ramm (1996): Constraint energy momentum algorithm and its application to nonlinear dynamics of shells, *Comp. Methods Appl. Mech. Eng.*, 136, 293-315.
- [19] Naghdi, P.M. (1972): The Theory of Shells and Plates. In *Encyclopedia of Physics* (edited by S. Flügge), Springer-Verlag.
- [20] Ramm, E. and Matzenmiller, A. (1986): Large deformation shell analyses based on the degeneration concept, In: *Finite Element Methods for Plate and Shell Structures, Vol. 1: Element Technology* (edited by T.J.R. Hughes and E. Hinton), Pineridge Press.
- [21] Sansour, C., Wriggers, P. and Sansour, J. (1997): Nonlinear dynamics of shells: theory, finite element formulation and integration schemes, *Nonlinear dynamics* 13: 279-305.
- [22] Simo, J.C.; Vu-Quoc, L. (1988): On the dynamics in space of rods undergoing large motions: a geometrically exact approach. *Comp. Meth. Appl. Mech. Eng.*, 66, 125-161.
- [23] Simo, J.C.; Fox, D.D. (1989): On a stress resultant geometrically exact shell model, Part I: Formulation and optimal parametrization. *Comp. Methods Appl. Mech. Eng.*, 72, 267-304.
- [24] Simo, J.C.; Tarnow, N. (1994): A new energy and momentum conserving algorithm for the non-linear dynamics of shells. *Int. J. Numer. Meth. Engng.*, 37, 2527-2549.
- [25] Zienkiewicz, O.C.; Taylor, R.L. (1989): *The Finite Element Method: Basic Formulation and Linear Problem*. McGraw-Hill.

Figure captions

- Figure 1: Base vectors in reference and current configuration.
- Figure 2: Commutative diagram of the shell-director velocities.
- Figure 3: Short cylinder: geometry and loading.
- Figure 4: Short cylinder: mid-surface displacements of a point initially lying at $(R, 0, 0)$.
- Figure 5: Short cylinder: mid-surface velocities of a point initially lying at $(R, 0, 0)$.
- Figure 6: Short cylinder: velocities of a shell-director initially positioned at $(R, 0, 0)$.
- Figure 7: Short cylinder: kinetic, potential and total energies.
- Figure 8: Spherical cup: geometry, material and loading conditions.
- Figure 9: Spherical cup: vertical displacement of node A ; Newmark scheme.
- Figure 10: Spherical cup: displacements of node A ; EC and EC schemes.
- Figure 11: Spherical cup: vertical component of mid-surface vertical velocity at node A .
- Figure 12: Spherical cup: velocity of a shell-director initially positioned at node A .
- Figure 13: Spherical cup: kinetic energy.
- Figure 14: Spherical cup: potential energy.
- Figure 15: Spherical cup: total energy.
- Figure 16: Spherical cup: vertical reaction at a node initially lying at $(R \sin \alpha_1, 0, 0)$.
- Figure 17: Spherical cup: time-step size.
- Figure 18: Spherical cup: sequence of configurations at $t = 0.9, 1.9, 2.3, 2.7, 2.9, 3.3, 5.0$.
- Figure 19: Ellipsoidal cup: geometry, material and loading conditions.
- Figure 20: Ellipsoidal cup: mid-surface displacements of node B .
- Figure 21: Ellipsoidal cup: bigger component of the total rotation of a shell-director initially positioned at node B .
- Figure 22: Ellipsoidal cup: kinetic energy.
- Figure 23: Ellipsoidal cup: potential energy.
- Figure 24: Ellipsoidal cup: total energy.
- Figure 25: Ellipsoidal cup: time-step size.
- Figure 26: Ellipsoidal cup: sequence of configurations at $t = 0.3, 0.75, 0.9, \approx 1.1, \approx 1.5$.

Table 1. Parameters of the shell-director rotation, velocity and acceleration, and related constraints.

	Material	Constraint	Spatial	Constraint
Rotation vector	$\boldsymbol{\vartheta}$	$\boldsymbol{\vartheta} \cdot \mathbf{e} = 0$	$\boldsymbol{\theta}$	$\boldsymbol{\theta} \cdot \mathbf{t} = 0$
Angular velocity	$\dot{\boldsymbol{\psi}}$	$\dot{\boldsymbol{\psi}} \cdot \mathbf{e} = 0$	$\dot{\boldsymbol{w}}$	$\dot{\boldsymbol{w}} \cdot \mathbf{t} = 0$
Angular acceleration	$\ddot{\boldsymbol{\psi}}$	$\ddot{\boldsymbol{\psi}} \cdot \mathbf{e} = 0$	$\ddot{\boldsymbol{w}}$	$\ddot{\boldsymbol{w}} \cdot \mathbf{t} = 0$
Rotation vector velocity	$\dot{\boldsymbol{\vartheta}}$	$\dot{\boldsymbol{\vartheta}} \cdot \mathbf{e} = 0$	$\dot{\boldsymbol{\theta}}$	see [8]
Rotation vector acceleration	$\ddot{\boldsymbol{\vartheta}}$	$\ddot{\boldsymbol{\vartheta}} \cdot \mathbf{e} = 0$	$\ddot{\boldsymbol{\theta}}$	see [8]

Table 2. Rotation parameters and updating schemes for the shell-director velocity and acceleration used in numerical examples.

Integration scheme	Rotation parameter	Evolution equations
Newmark (N); "version 1"	incremental, material: $\boldsymbol{\vartheta}_{n+1}$	(4.14), (4.15) with (4.2)
Newmark (N); "version 2"	incremental, material: $\boldsymbol{\vartheta}_{n+1}$	(4.18), (4.19)
Energy conserving (EC)	total, material: $\boldsymbol{\vartheta}$	(4.26)
Energy decaying (ED)	total, material: $\boldsymbol{\vartheta}$	(4.44)

Table 3. Short cylinder: Loading data.

Angle α	0	$\pi/2$	π	$3\pi/2$
Nodal loads	$\begin{Bmatrix} 0 \\ -1 \\ -1 \end{Bmatrix} p(t)$	$\begin{Bmatrix} 1 \\ 1 \\ 1 \end{Bmatrix} p(t)$	$\begin{Bmatrix} 1 \\ 1 \\ 1 \end{Bmatrix} p(t)$	$\begin{Bmatrix} 0 \\ -1 \\ -1 \end{Bmatrix} p(t)$

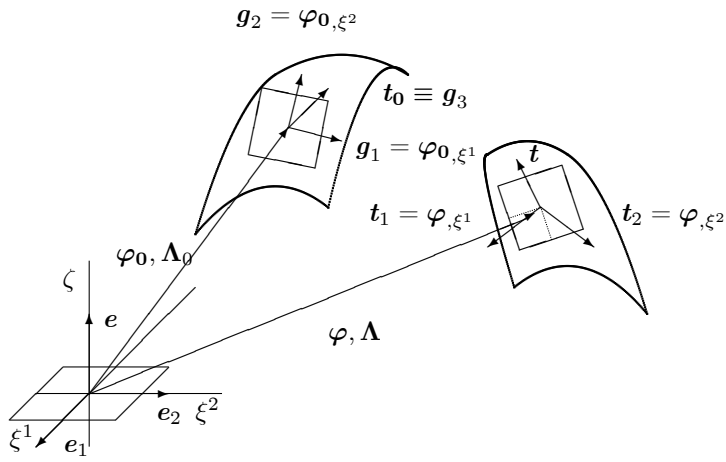


Figure 6.1: This is Figure 1

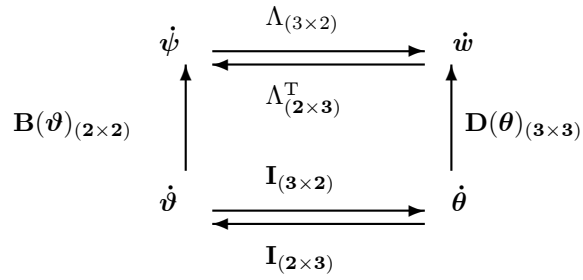


Figure 6.2: This is Figure 2.

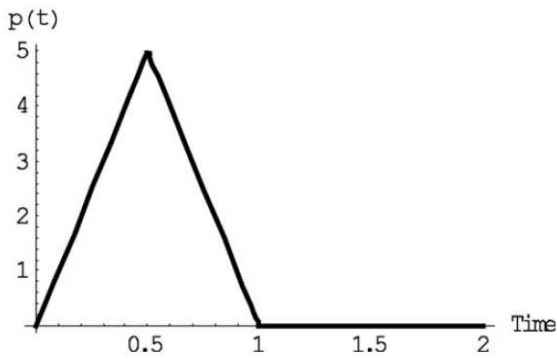
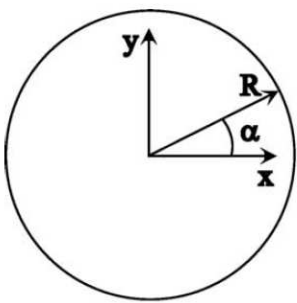


Fig. 3. Short cylinder: geometry and loading.

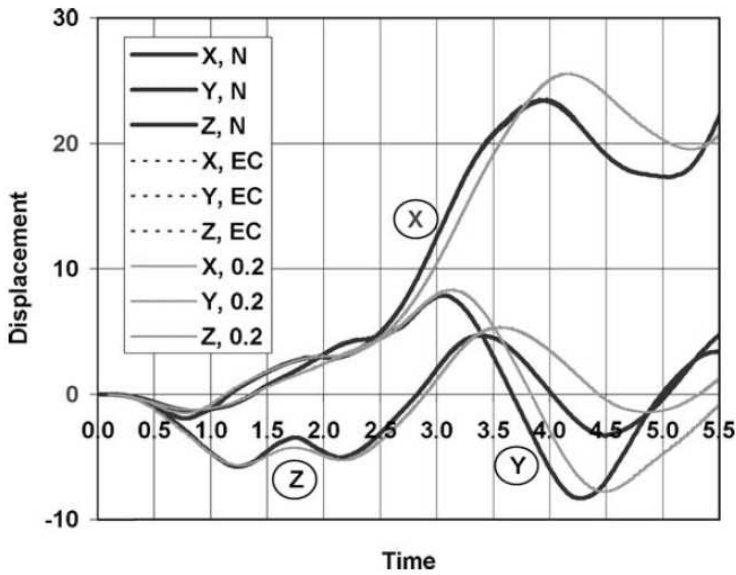


Fig. 4. Short cylinder: mid-surface displacements of a point initially lying at $(R, 0, 0)$.

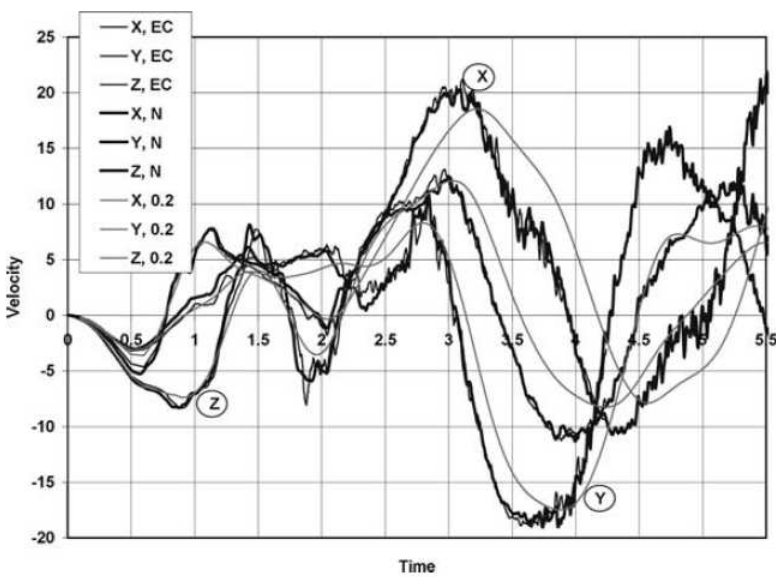


Fig. 5. Short cylinder: mid-surface velocities of a point initially lying at $(R, 0, 0)$.

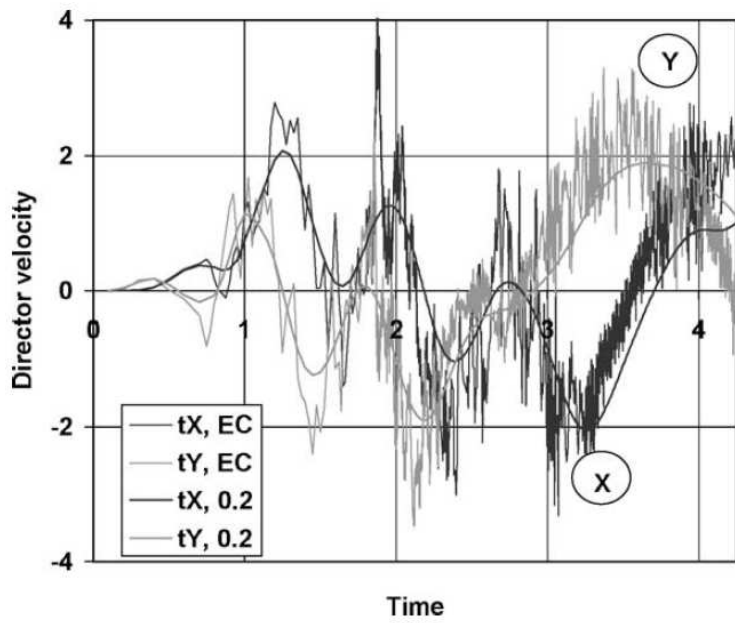


Fig. 6. Short cylinder: velocities of a shell-director initially positioned at $(R, 0, 0)$.

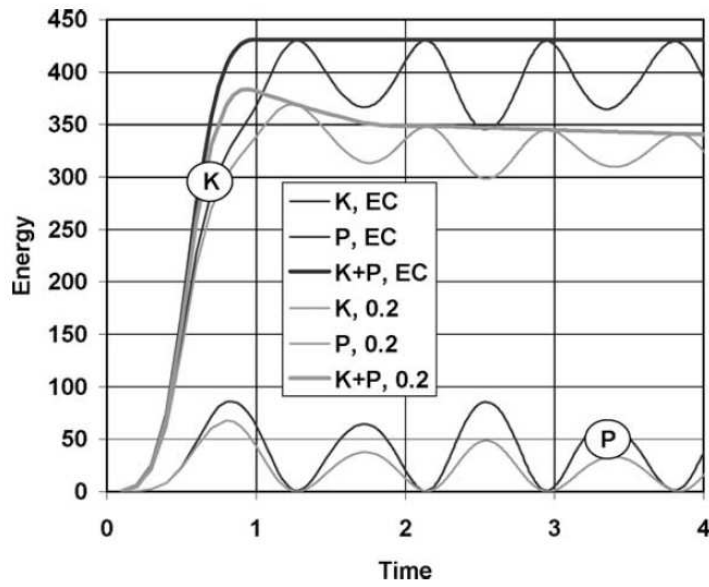


Fig. 7. Short cylinder: kinetic, potential and total energies.

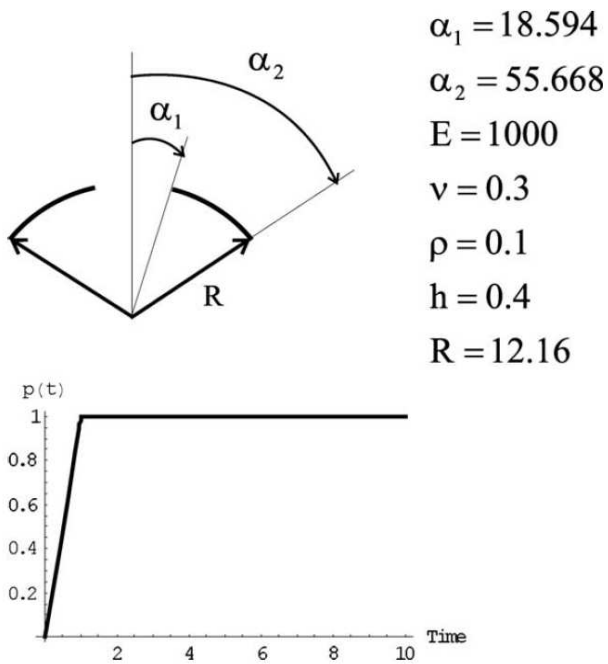


Fig. 8. Spherical cup: geometry, material and loading conditions.

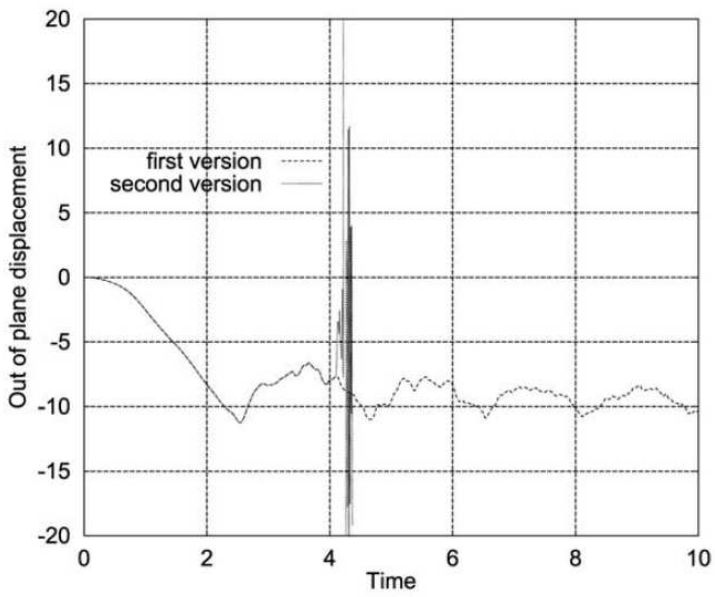


Fig. 9. Spherical cup: vertical displacement of node *A*; Newmark scheme.

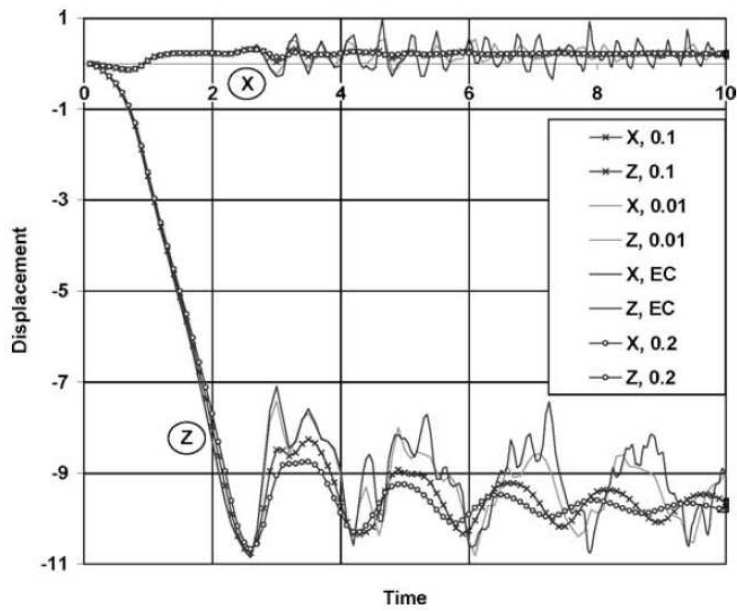


Fig. 10. Spherical cup: displacements of node *A*; EC and EC schemes.

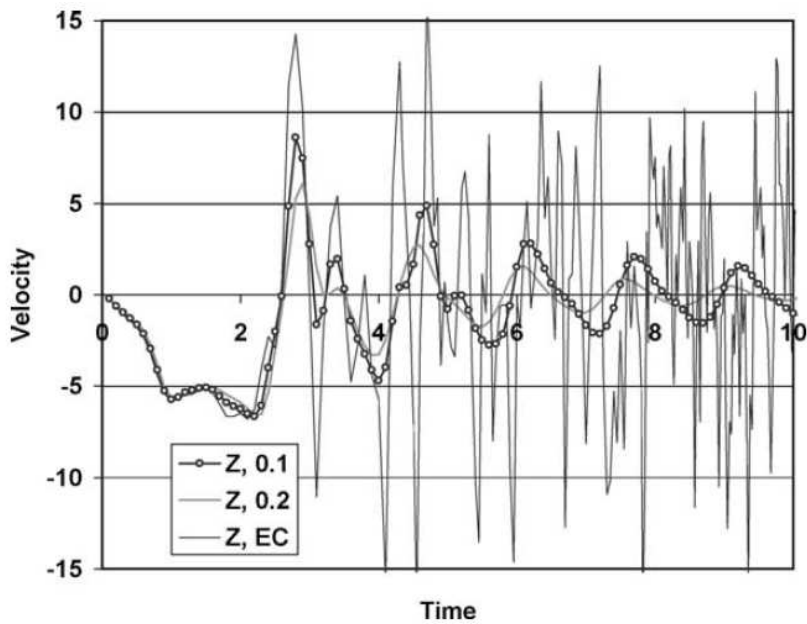


Fig. 11. Spherical cup: vertical component of mid-surface vertical velocity at node *A*.

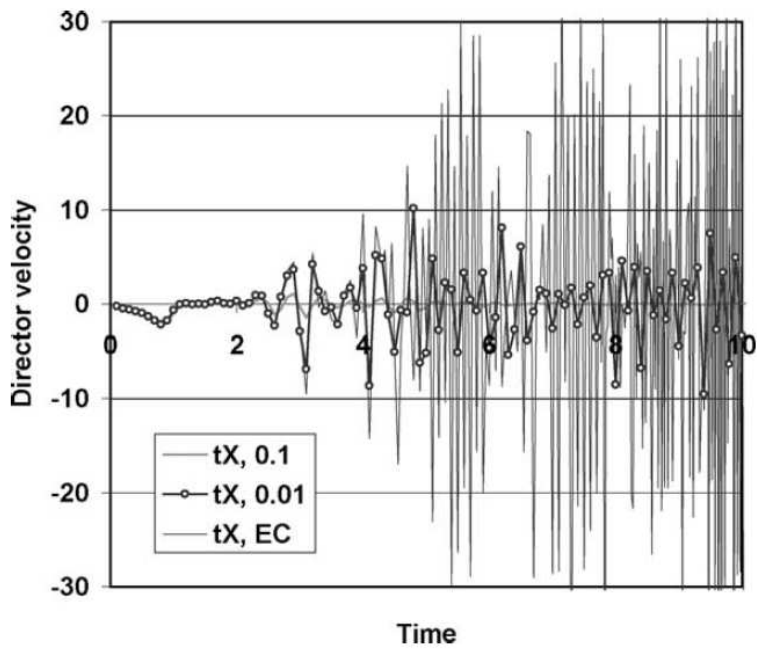


Fig. 12. Spherical cup: velocity of a shell-director initially positioned at node A .

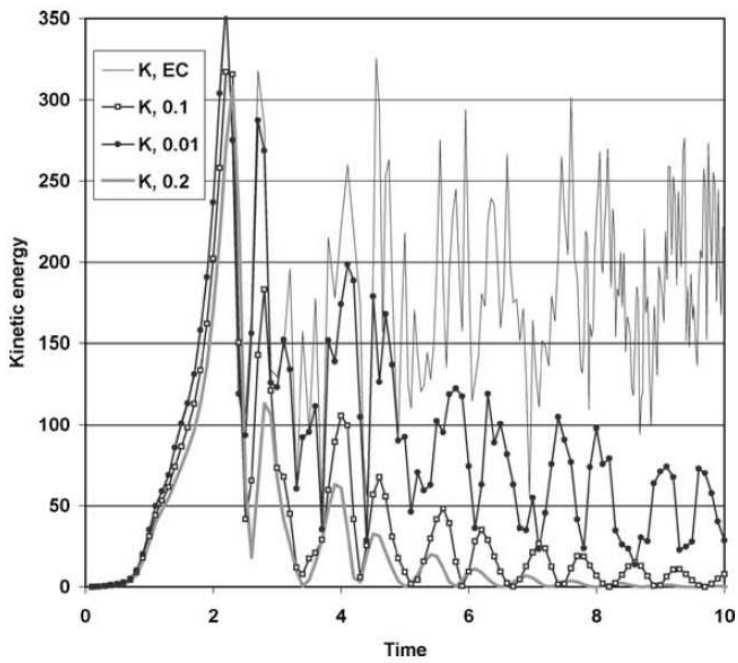


Fig. 13. Spherical cup: kinetic energy.

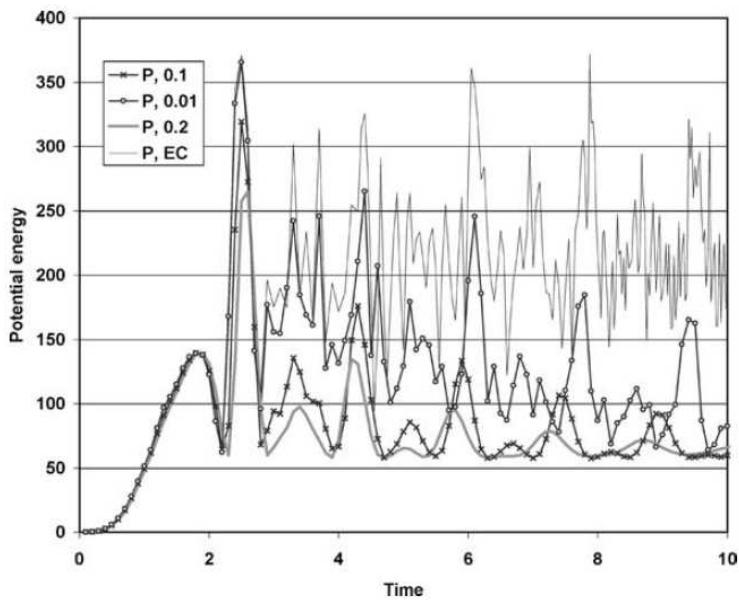


Fig. 14. Spherical cup: potential energy.

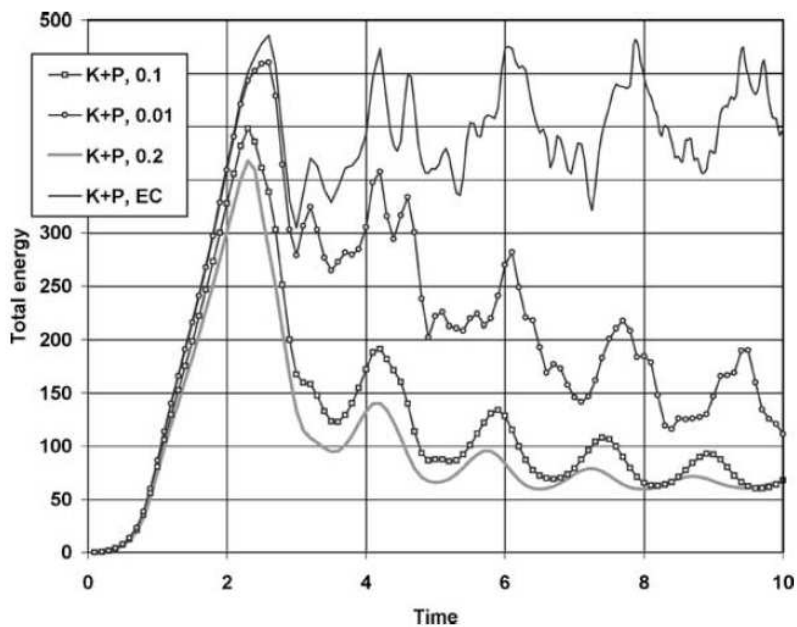


Fig. 15. Spherical cup: total energy.

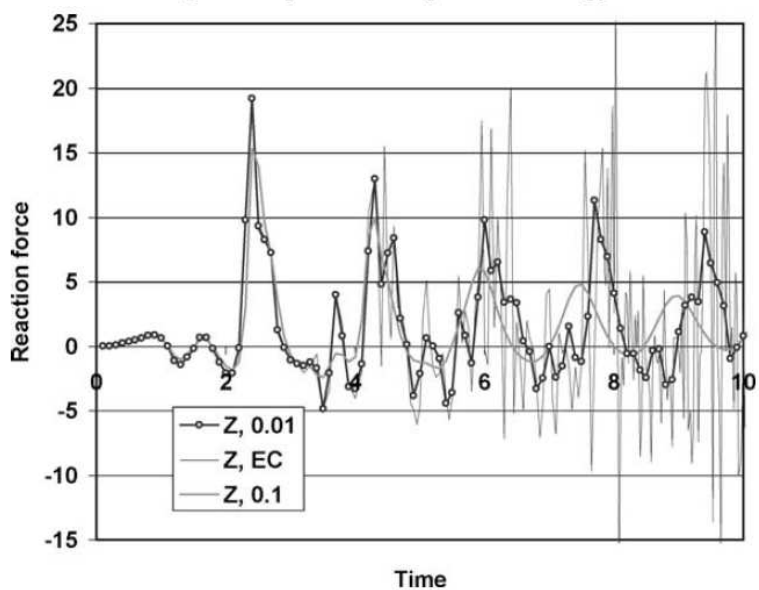


Fig. 16. Spherical cup: vertical reaction at a node initially lying at $(R \sin \alpha_1, 0, 0)$.

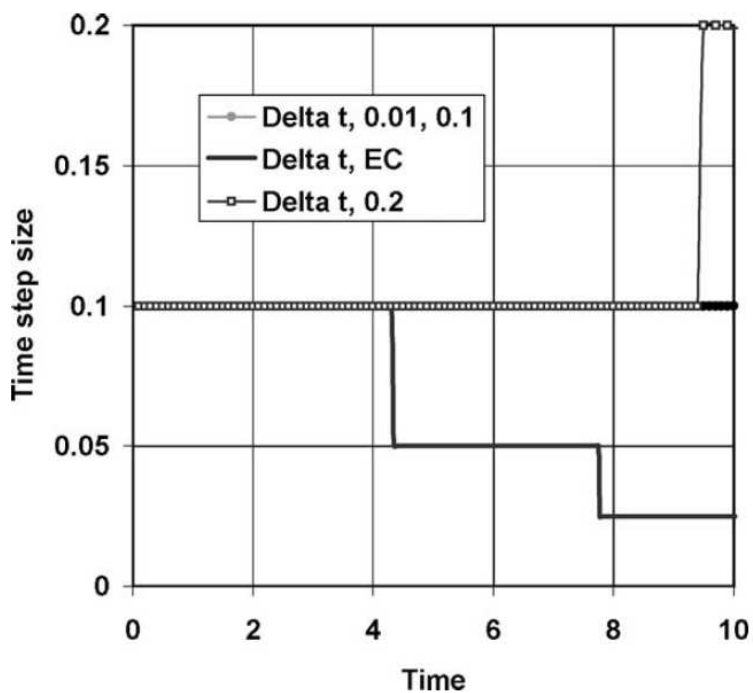


Fig. 17. Spherical cup: time-step size.

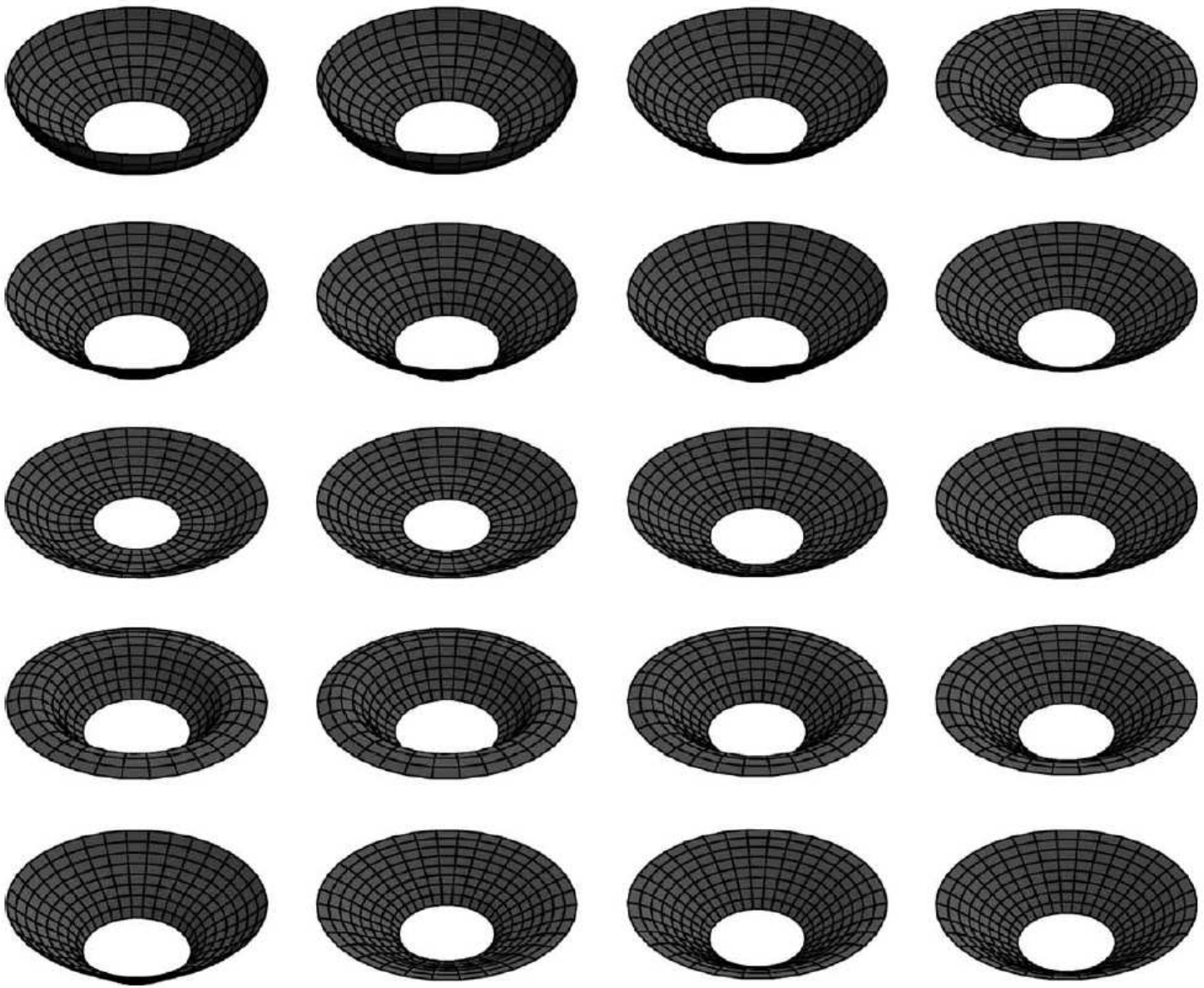
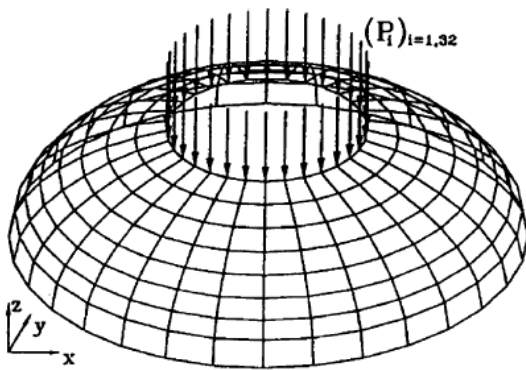


Fig. 18. Spherical cup: sequence of configurations at $t = 0.9, 1.9, 2.3, 2.7, 2.9, 3.3, 5.0$.



$(P_i)_{i=1,32}$
R_{max}: 10
R_{min}: 3.88
Height: 4.60
Thickness: 0.4
Modulus E: 1000
Modulus ν : 0.3
Density: 0.0001

Time	$p(t)$
0.00	0.00
1.00	1.60
1.07	1.65
1.16	1.65
1.20	1.60
1.94	0.05
2.00	0.00

$$(P_i)_{i=1,32} = [0, 0, -1]^T p(t)$$

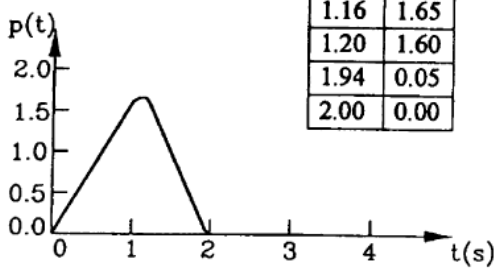


Fig. 19. Ellipsoidal cup: geometry, material and loading conditions.

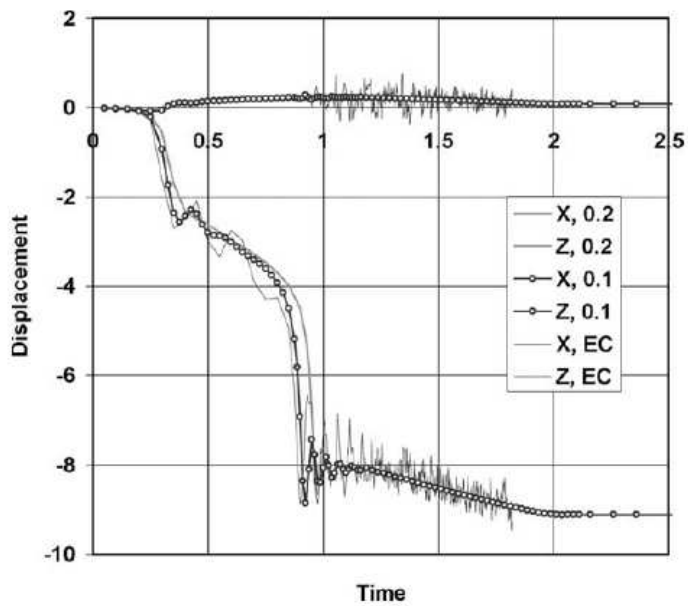


Fig. 20. Ellipsoidal cup: mid-surface displacements of node *B*.

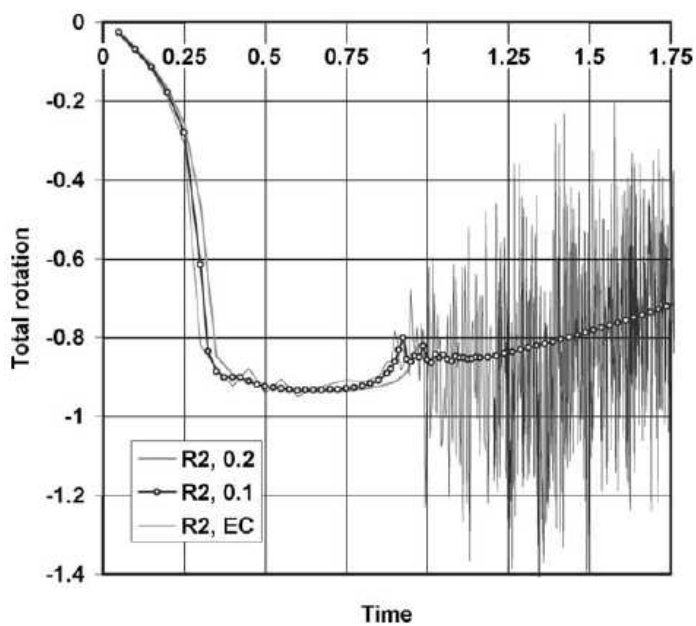


Fig. 21. Ellipsoidal cup: bigger component of the total rotation of a shell-director initially positioned at node *B*.

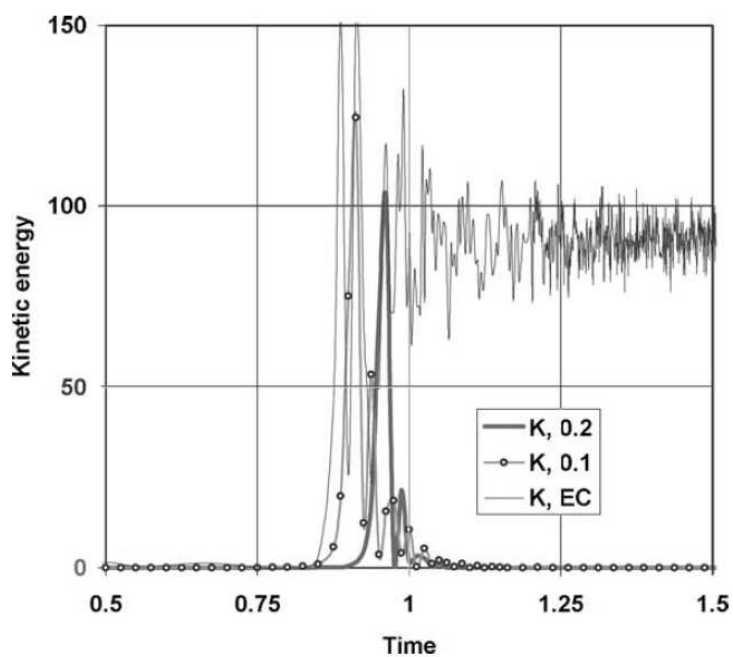


Fig. 22. Ellipsoidal cup: kinetic energy.

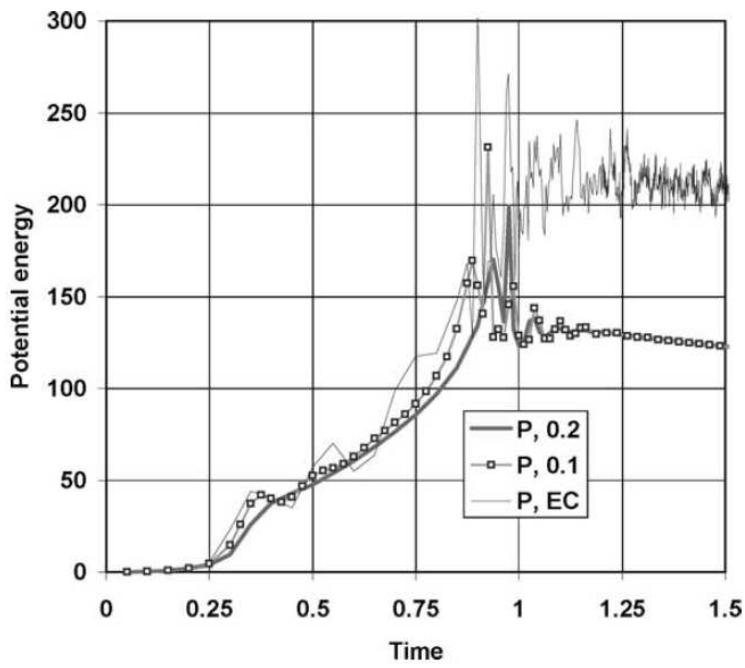


Fig. 23. Ellipsoidal cup: potential energy.

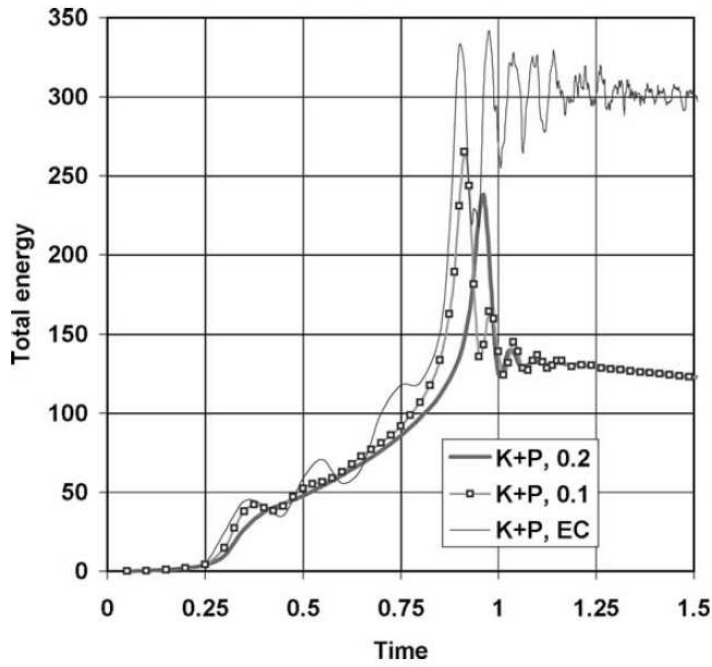


Fig. 24. Ellipsoidal cup: total energy.

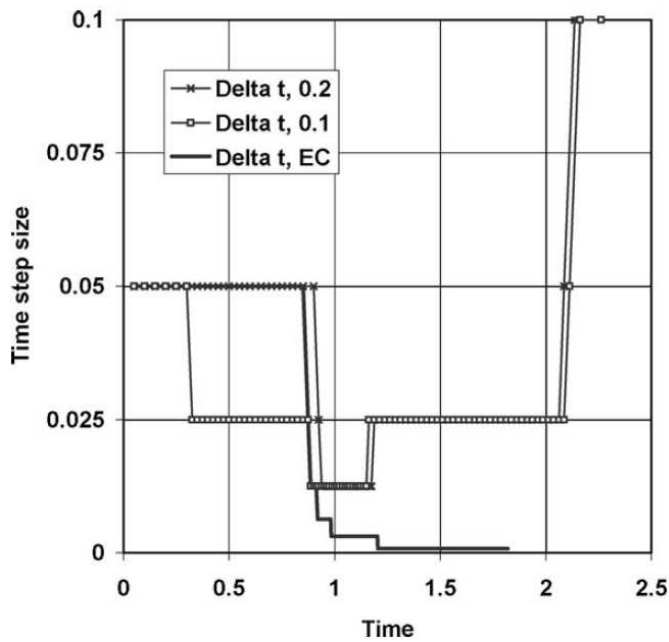


Fig. 25. Ellipsoidal cup: time-step size.

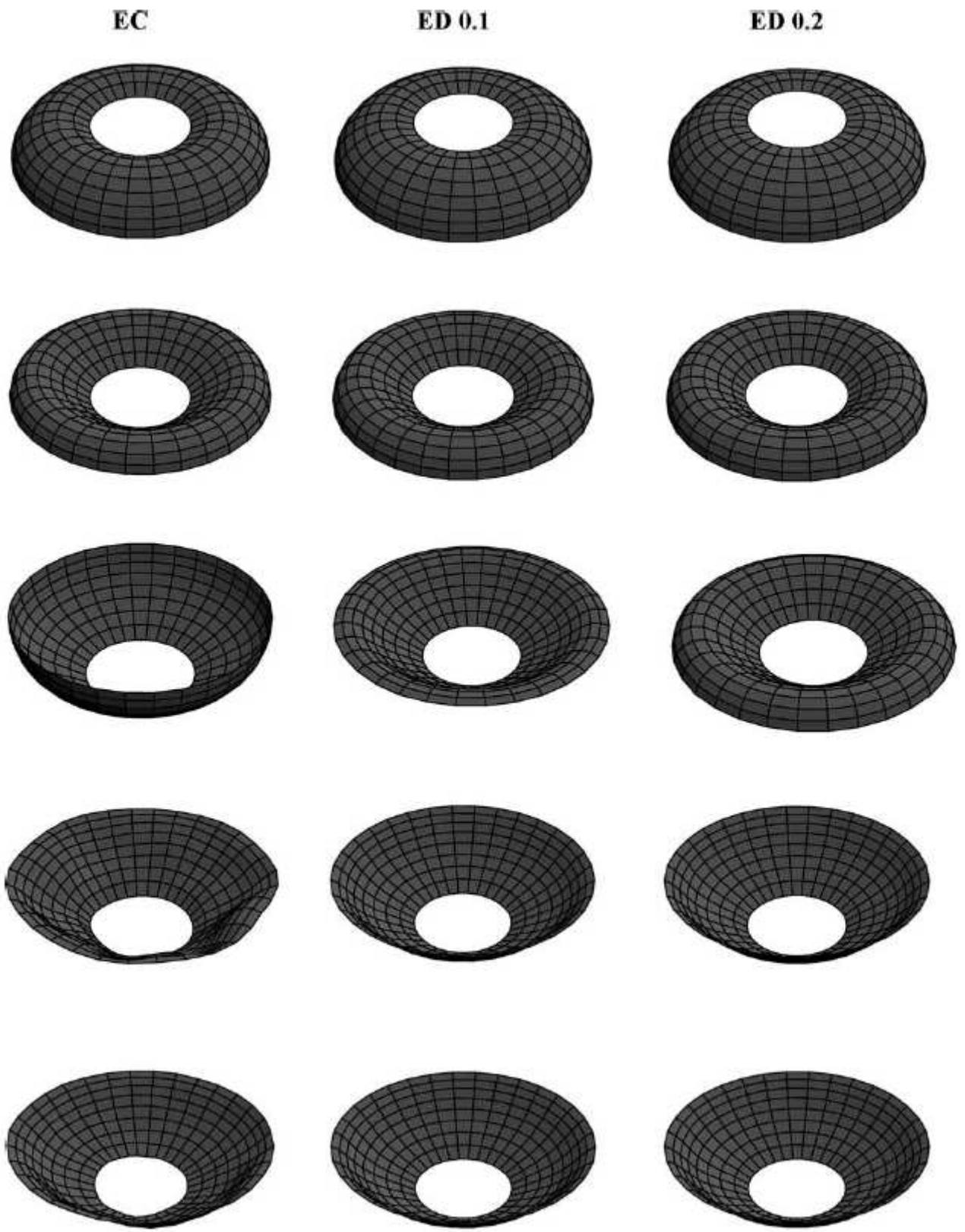


Fig. 26. Ellipsoidal cup: sequence of configurations at $t = 0.3, 0.75, 0.9, \approx 1.1, \approx 1.5$.